Revision 2

The relationship between REE-Y-Nb-Th minerals and the evolution of an A-type granite, Wentworth Pluton, Nova Scotia

Angeliki D. Papoutsa and Georgia Pe-Piper

Department of Geology, Saint Mary's University, Halifax, Nova Scotia B3H 3C3, Canada

ABSTRACT

The Wentworth Pluton in the Eastern Cobequid Highlands consists principally of metaluminous to peralkaline A-type granite (~362 Ma), a large part of which was remelted by a major gabbro intrusion (~357 Ma). Magmatic minerals like allanite-(Ce), chevkinite-(Ce), zircon, and hingganite-(Y) and post-magmatic mineral phases, such as REE-bearing epidote, samarskite-(Y), aeschynite-(Y), fersmite, thorite-like phases, and hydroxylbastnäsite-(Ce), were identified. The presence of fluorine in the parental magma, indicated by whole-rock geochemical data and the presence of fluorite, increased the solubility of monazite and xenotime and thus facilitated retainment of rare metals in the magmatic system. Fractionation of allanite-(Ce) and chevkinite-(Ce) led to a melt enriched in heavy rare earth elements (HREE), from which hingganite-(Y) crystallized during late magmatic stages. The remelting of the early granite led to fluorine and sulfur release in volatile phases, which circulated with hydrothermal fluids, thus mobilizing the REE and other rare metals. Reduction of fluorine activity during the late to post-solidus crystallization resulted in the precipitation of HREE and rare metals in samarskite-(Y), thereby enriching the residual hydrothermal fluids in light rare earth elements (LREE). Post-magmatic LREE minerals, such as hydroxylbastnäsite-(Ce), either replaced earlier minerals or precipitated from these hydrothermal fluids. Carbonate fluids involved in a late regional hydrothermal circulation event along the Cobequid-Chedabucto fault (320-315 Ma) promoted Ti mobility and the formation of TiO_2 minerals and probably of aeschynite-(Y). This mineralogical diversity, in

addition to the complex geological history of the pluton, provides a unique opportunity to correlate the formation of individual rare-metal minerals to different stages of pluton evolution and thus provide an insight to the formation conditions of these minerals.

Keywords: A-type, geochemistry, Wentworth pluton, REE-minerals, anatexis

INTRODUCTION

A-type granites usually occur in extensional settings and have a distinct alkaline geochemical signature. Enrichment in rare-earth elements (REE) and other rare metals, such as Y, Nb, Ta, Th and U, is common in these rocks. Rare-earth minerals like allanite, monazite, chevkinite, xenotime, cerite, synchysite and gadolinite are commonly found in A-type granites worldwide (Förster 2000; Wood and Ricketts 2000; Jiang 2006; Vlach and Gualda 2007; Saveleva and Karmanov 2008).

Accessory minerals in granitic rocks are essential carriers of rare metals. Their internal zoning, compositional variations and patterns of alteration provide a valuable source of information concerning the magmatic and post-magmatic evolution of their host rocks including fractionation, rock-fluid interaction and metamorphic overprint (Uher et al. 2009). Accessory minerals in granitic rocks typically show more chemical and textural variability than the major minerals. Their crystallization is sensitive to various environmental parameters and therefore they are a useful indicator of the magmatic history of their host rock (Wang et al. 2001).

The Wentworth pluton is known to host REE mineralization (MacHattie 2009). The granites and their volcanic equivalents in the northeastern part of the intrusion are generally enriched in F and U (Gower 1988). Associated mineralization includes fluorite-zircon-titanite-calcite-allanite veins, with highly anomalous REE concentrations, hosted by the granite (Gower 1988).

The variety of rare-metal minerals in the Wentworth pluton is unusual. The occurrences of Nb-REE-Y oxides in A-type granites worldwide and the understanding of their formation conditions are still limited. The complex geological history of this pluton provides a unique opportunity to correlate mineral assemblages to magmatic evolution. The purpose of this study is to identify and characterize the rare-metal minerals present at Wentworth and relate their textural features to the evolutionary history of their host rocks. Comparison of the whole-rock and mineral chemistry is then used to infer the formation conditions of these minerals.

GEOLOGICAL SETTING

The Cobequid Highlands are located in the southern part of the Canadian Appalachians, just north of the boundary between the Avalon and Meguma terranes (Calder 1998; Pe-Piper and Piper 2002). This boundary is marked by the Cobequid-Chedabucto fault zone, along which strike-slip motion took place during the Late Paleozoic (Murphy et al. 2011). In the Late Devonian and Early Carboniferous, granite plutons with lesser gabbros intruded along a regional shear zone that encompassed the entire Cobequid Highlands (Pe-Piper 2007). Coeval volcanism in the Cobequid Highlands is represented by felsic pyroclastic rocks (Byers Brook Formation) that are geochemically similar to the granites, and by basalt flows (Diamond Brook Formation) that are geochemically similar to the gabbros in the Wentworth pluton (Dessureau et al. 2000).

The Wentworth pluton is located in the eastern part of the Cobequid Highlands (Fig.1a). The northeastern part of the pluton consists of the Hart Lake-Byers Lake (HLBL) granite, which is separated from the Folly Lake gabbro in the southwest by a zone in which younger granite and gabbro are predominant (Koukouvelas et al. 2002). The Wentworth pluton includes all of the granite and gabbro phases (Fig. 1b).

Field relationships show that the Folly Lake gabbro is younger than the HLBL granite (Koukouvelas et al. 2002). A hornblende sample from the Folly Lake gabbro yielded an $^{40}Ar/^{39}Ar$ age of 357±4 Ma (Pe-Piper et al. 2004; Murphy et al. 2011), whereas a zircon sample from the HLBL granite has yielded a U-Pb age of 362±2 Ma (Doig et al. 1996) (Fig. 1c).

The age of the equivalent volcanic rocks is constrained by U-Pb zircon ages of 358±1 Ma from the top of the Byers Brook Formation and 355±3 Ma from the middle of the Diamond Brook Formation (Fig. 1c). Palynomorphs show that minor interbedded sediment in the Byers Brook Formation is of late Famennian age and in the Diamond Brook Formation is of mid-Tournaisian age (Dunning et al. 2002) (Fig. 1c).

Part of the granite near the Folly Lake gabbro of the Wentworth pluton was evidently remelted, resulting in bodies of "late" granite with slightly different compositions from the HLBL granite. Some of these bodies have textures indicating magma mixing with gabbro (Pe-Piper 2007). The Folly Lake gabbro consists of gabbro–diorite cut by this "late" medium-grained granite in globular pods, irregular sheets, net-veined complexes, and linear dykes, some of which are pegmatitic. Mafic enclaves are common in the granites and some show mixing and mingling at the contact with the granite (Koukouvelas et al. 2002).

The southern margin of the Wentworth pluton is in direct contact with the Rockland Brook Fault (Fig. 1b), which was a major dextral shear zone at the time of pluton emplacement (Miller et al. 1995; Koukouvelas et al. 2002). Syn-magmatic deformation of the Wentworth pluton is widespread, and almost all major contacts of different units in the pluton were active faults (Koukouvelas et al. 2002). The plutonic complex was compartmentalized into smaller blocks with faults parallel to the Rockland Brook Fault during the final stages of emplacement. Between 315 and 320 Ma, there was a major phase of faulting and mineralization associated with

93 E-W movements along the Chedabucto fault (Fig. 1a) and its continuation along the Cobequid
94 Fault (Murphy et al. 2011).

95 **THE WENTWORTH GRANITES**

96 The Wentworth granites are fine- to coarse-grained monzogranites and syenogranites (Pe-
97 Piper 2007). Individual samples may be amphibole-, amphibole-biotite or biotite-bearing.
98 Amphiboles are sodic, sodic-calcic or calcic, any of which can coexist with biotite. Most granites
99 are equigranular, however some samples are porphyritic or granophyric (interpreted as high level
100 granites). Most granite samples of the Wentworth pluton show brittle deformation and alteration
101 is represented by secondary minerals (white mica, epidote, quartz, albite, chlorite, actinolite and
102 riebeckite). Hydrothermal quartz, fluorite and epidote are also present in veinlets.

103 The A-type granite of the Wentworth pluton is the most alkaline of a series of Late
104 Paleozoic metaluminous to mildly peralkaline (Fig. 2) plutons along the Cobequid shear zone
105 (Pe-Piper 2007). The Shand's index [(ANK) = molar (Al_2O_3/(Na_2O+K_2O); Maniar and Picolli
106 1989] of the Wentworth Pluton granites ranges between 0.8 to 1.16, i.e. straddling to the
107 boundary between metaluminous and peralkaline compositions (Table 1, Fig. 2).

108 The HLBL granite, the early phase of the Wentworth Pluton, has a composition of about
109 76% SiO_2, high F (>500 ppm) and moderate Li (>20 ppm) contents (Koukouvelas et al. 2002).
110 This early granite shows subtle differences in bulk geochemistry from the syn- and post-gabbro
111 granites: for the same SiO_2 content, TiO_2 is lower, whereas F and Nb tend to be higher in the
112 early granite (Koukouvelas et al. 2002; Pe-Piper 2007). A few varieties of granite, interpreted as
113 synchronous with the gabbro on the basis of lobate contacts, have particularly high Zr contents.
114 Many of syn- and post-gabbro granites are alkalic, with >75 ppm Y. Some have high Li, but all
115 have <400 ppm F (Koukouvelas et al. 2002). Some granites that occur as pods within the gabbro

are geochemically distinct, with a wide range of SiO_2 contents, relatively low F and the amphibole, where present, is hornblende. Their particularly low F may indicate that melting of the early granite by the gabbro resulted in the release of F in a volatile phase (Koukouvelas et al. 2002).

ANALYTICAL METHODS AND SAMPLES

The location of the samples was indicated on the 1:50000 maps of Pe-Piper and Piper (2005). The studied samples are attributed to different types according to their location and field relations with the gabbro (Table 1). Uniform outcrops of granite cut by gabbro are considered to be of the early granitic phase (HLBL granite). Granites with lobate contacts with the gabbro and hybrid enclaves are interpreted as synchronous with the mafic intrusion. Bodies of granite that either cut the Folly Lake gabbro or occur in it as globular pods or irregular sheets are considered to be of the late granitic phase. Where field relations were clear, sample attribution is characterized as “definite” .Where the relative age of a sample could not be clearly defined from its field relations in the same outcrop, but was assumed from the geology of nearby outcrops, the sample attribution was classified as “probable”.

A total of 40 thin and 57 polished sections were first examined with a petrographic microscope using polarized and reflected light, in order to determine the mineralogy and the textures of these samples. Minerals that could not be identified using the petrographic microscope were analyzed in carbon-coated slides by energy dispersive spectroscopy (EDS) using a LEO 1450 VP SME scanning electron microscope with a maximum resolution of 3.5 nm at 30 kV. The EDS analyses were used to qualitatively identify groups of minerals that were further analyzed using a JEOL-8200 electron microprobe equipped with five wavelength spectrometers and a Noran 133 eV energy dispersion detector. The operating conditions were on

accelerating voltage of 15kV, a beam current of 20nA and a beam diameter of 1µm. Part of microprobe analysis routine includes dealing with peak interference, i.e. Er-Nb, Ti-Hf, Zr-P, Hf-Ho, Er-Hf, Hf-Er and F-Ce. The apparent peak intensities corresponding to these elements were measured in standards that do not contain the elements with overlapping peaks. Using these intensities, peak-overlap correction factors were calculated to estimate the real concentrations of measured elements. From the 57 polished sections that were examined, only 12 samples contain rare-metal minerals.

SILICATE MINERALS

Allanite-(Ce) and REE-bearing epidote

Allanite-(Ce) is found principally in the HLBL granite but also in some late granites (Table 1). In thin section, allanite-(Ce) appears dark yellow to brown and occurs as large euhedral, isolated crystals (Figs. 3a and 3b) and as inclusions in amphibole crystals (Figs. 3c and 3d). Most of the allanite-(Ce) grains are inhomogeneous and some exhibit growth and irregular zoning in polarized light and back-scattered-electron (BSE) images. Electron-microprobe analyses (Table 2) of euhedral, discrete grains show a total of about 20 wt% REE, 10 wt% FeOt, 10 wt% Al_2O_3 and 8 wt% CaO. Rare-earth patterns for allanite-(Ce) show enrichment in light REE (LREE) relative to heavy REE (HREE), with a positive Eu anomaly (Fig. 4a).

Anhedral overgrowths and interstitial grains that look optically similar to allanite-(Ce) were also analyzed. These show lower amounts of LREE (15 wt%) and higher amounts of CaO (15 wt%), FeOt (18 wt%) and Al_2O_3 (15-20 wt%) (Table 2) compared with analyses of euhedral allanite-(Ce), and are classified as REE-rich epidote based on the nomenclature of Armbruster et al. (2006).

Chevkinite-(Ce)

The composition of the grains reported here plot in the chevkinite field of the discrimination diagram proposed by Macdonald et al. (2002).Chevkinite-(Ce) occurs in four granite samples that appear to be synchronous with, or post date, the gabbroic intrusion (Table 1). In thin section, most chevkinite-(Ce) forms dark red, close to opaque, euhedral crystals associated with zircon, Fe-Ti oxides, feldspar and quartz (Figs. 5a and 5b). Some amphibole grains contain inclusions of chevkinite-(Ce) (Figs. 5c and 5d) and a grain of primary ferro-edenite forms an interlocking texture with chevkinite-(Ce) (Fig. 5e and f).

Chevkinite-(Ce) is enriched in LREE, particularly Ce_2O_3 (20 wt%), and contains moderate ThO_2 (up to 5 wt %) and Nb_2O_5 (up to 4.6 wt%) contents (Table 3). The main characteristics of REE patterns for chevkinite-(Ce) are similar to those described for allanite-(Ce) but the REE concentrations are higher in the former mineral. LREE are enriched relative to HREE with a positive Eu anomaly (Fig. 4b). Chevkinite-(Ce) patterns exhibit less variation than those of allanite-(Ce); only the La contents show small variations. In places, chevkinite-(Ce) crystals are surrounded by a yellowish, continuous rim (Figs. 5a-f) and the core appears corroded (Figs. 5e and 5f). Electron-microprobe analyses indicate that this yellow mineral is also chevkinite-(Ce) but is depleted in LREE and enriched in Ti and Fe relative to the core (Table 3, analysis 122).

Altered (?) chevkinite-(Ce)

A crystal of an Fe-rich mineral was found in syn-gabbro granite (sample 6490). The crystal is strongly fractured and appears inhomogeneous. Fractures within this grain do not continue or cross-cut adjacent grains, suggesting that they are not of tectonic origin but stem from a change in volume during mineral replacement. X-ray compositional mapping (Fig. 6) shows that, although this mineral is optically similar to chevkinite-(Ce), there are significant

compositional differences between them. The Fe concentration is three times higher (30 wt %) in the unidentified mineral than in the chevkinite-(Ce), whereas its REE contents are lower. A Ce map shows a randomly distributed high-concentration areas throughout the grain (Fig. 6a); these areas could be remnants of what was once a Ce-rich phase, but is now completely altered. The high-Ce areas correspond to areas of low Fe content (Fig. 6b). Electron-microprobe analyses show large chemical variations even over distances of a few microns, with very low totals, making the identification of individual phases impossible. Titanium levels are higher in the core, which is the most fractured part of the grain (Fig. 6c) and generally correlate with areas of low Ca (Fig. 6d). This grain is also tentatively identified as altered chevkinite-(Ce) on the basis of its optical properties and the absence of other large euhedral REE-Fe-Ti-rich accessory minerals in the examined samples.

Zircon

Zircon is a common accessory mineral in the studied granites. Most zircon crystals are euhedral. Some are optically and compositionally zoned, with Hf showing a large variation (Table 4). Zircon crystals in HLBL granite sample 9832 are turbid, appear fractured and contain inclusions rich in Th (Figs. 7a and 7b). Zircon in sample 6518 is bounded by fractures and has an optically clear core surrounded by a turbid, discontinuous, fractured, porous zircon depleted in Zr and enriched in Th (Figs. 7c-e). This overgrowth is relatively rich in Y_2O_3 (up to 3.6 wt%), HfO_2 (up to 2.6 wt%) and ThO_2 (Table 4). All analyzed zircon crystals contain low levels of REE, particularly the medium and heavy REE.

Hingganite-(Y)

Hingganite-(Y) is found in only one sample of post-gabbro granite (6419, Table 1). In thin section, it has similar optical properties to zircon but appears brighter in the BSE images.

Two grains of hingganite-(Y) were identified, and both are adjacent to a much larger grain of secondary allanite-(Ce), which occurs in association with an unknown alteration mineral (Figs. 8a and 8b). The hingganite-(Y) contains up to 31 wt. % Y_2O_3 and is enriched in middle REE, and particularly Gd and Dy, relative to the remaining REE (Fig. 4c). Rare-earth patterns show a negative Eu anomaly and a slight depletion of LREE relative to HREE (Fig. 4c). Hingganite-(Y) grains are zoned showing a slight rimward depletion in Y and enrichment in Ce (Table 5, analyses 145 and 146). Low totals (≤ 87%) are attributed to the undetermined Be and H_2O contents.

Thorite-like phase

A phase stoichiometrically approaching thorite was found in one sample of syn-gabbro granite (6490) as a small independent grain (10 μm) showing an interlocking texture with zircon (Fig. 9a). It is enriched in FeOt (9.4 wt%), Nb_2O_5 (7.7 wt%) and shows moderate enrichment in Y_2O_3 (2.1 wt%). Low levels of REE (<1 wt. %) are also present (Table 6).

OXIDE MINERALS

Samarskite-(Y)

Samarskite-(Y) is an Y-rich Nb-oxide found in four of the studied samples of various ages (Table 1). Samarskite-(Y) occurs both as isolated (Fig. 9a) euhedral rhombic crystals (sample 9827A; Figs. 9b and 9c) and as intergrowths with another Nb-oxide, fersmite (Figs. 9d and 9e). In thin section, euhedral crystals of samarskite-(Y) are yellow to pale green (Fig. 9b). One of the crystals (sample 9827A) contains an inclusion of euhedral zircon (Figs. 9b and 9c). The mineral is classified as samarskite-(Y) based on the strong dominance of Y over REE (Table 7). It contains up to 25 wt% Y_2O_3 and 53 wt% Nb_2O_5, and almost equal proportion of Gd_2O_3 and Dy_2O_3 (3-5 wt%). The HREE are represented mostly by Yb and LREE are dominated by Nd (up

231 to 4 wt% Nd_2O_3; Table 7). The REE patterns of samarskite-(Y) show a negative Eu anomaly and
232 HREE enrichment relative to the LREE (Fig 4d).

233 **Fersmite**

234 Fersmite grains were found in four samples, principally from the HLBL granite (Table 1).
235 Fersmite occurs as small (<10 μm) isolated grains (sample 4636), as inclusions in fluorite
236 developed between fractured feldspar crystals (sample 7658; Figs. 11a and 11b), and in
237 association with samarskite (samples 9831 and 9832; Figs. 10c and 10d). Grains consisting of
238 fersmite and samarskite are dark brown and turbid. Electron-microprobe analyses (Table 7) show
239 that samarskite-(Y) and fersmite contain comparable levels of niobium, but fersmite is depleted
240 in Y (5.5 wt% Y_2O_3) and enriched in U and Th (6.3 and 13 wt% respective oxides). Fersmite is
241 also enriched in LREE and particularly Ce (ca. 4 wt% Ce_2O_3; Table 8), whereas samarskite-(Y)
242 has high concentrations of middle and heavy REE (Fig. 4e).

243 **Aeschynite/Polycrase-(Y)**

244 This Y-rich mineral was identified in a single sample of the HLBL granite (9832). In thin
245 section, it is dark brown and turbid (Figs. 11a and 11b). It is associated with clots of titanite
246 grains, a TiO_2 mineral and secondary REE-rich epidote, and in some cases occurs in fractures. In
247 places, aeschynite-(Y) appears to enclose titanite grains (Fig. 11b). Electron-microprobe analyses
248 (Table 8) show that TiO_2, Y_2O_3 and Nb_2O_5 are the major components (42 wt%, 23 wt% and 12
249 wt% respectively). It is moderately enriched in middle REE, particularly Gd and Dy (3.8 wt%
250 and 4.8 wt% respective oxides) and contains lower levels of LREE and HREE (Table 8; Fig. 4f).
251 Stoichiometrically, this mineral matches either aeschynite-(Y) or polycrase-(Y). However, Th is
252 more abundant than U, which is characteristic of the aeschynite group minerals (Ewing 1975).
253 Furthermore, the analyzed grains are enriched in HREE relative to LREE (Table 8), which is

another characteristic of the aeschynite group (Škoda and Novák 2007). However due to the metamict nature of these minerals and their minor chemical differences, their true identity cannot be ascertained on the basis of WDS data alone. In the present study, we will refer to this mineral as aeschynite-(Y).

TiO_2 mineral

A single grain of TiO_2 phase was found in one sample from the HLBL granite (9832). It is dark brown, almost opaque, bounded by fractures and is associated with a clot of titanite grains hosting aeschynite-(Y) (Figs. 11a and 11b). It contains 2.8 wt% Nb_2O_5, traces of Fe, Ca and Ta, but is almost completely devoid of REE (Table 8). Due to the lack of XRD data, we cannot determine whether this phase is rutile, anatase or brookite.

CARBONATE MINERALS

Hydroxylbastnäsite-(Ce)

Hydroxylbastnäsite-(Ce) is a REE carbonate mineral which was found in one sample of granite intruding the Byers Brook Formation (7658). This mineral formed around the rim of a euhedral crystal of allanite-(Ce) (Fig. 3b). In thin section, hydroxylbastnäsite-(Ce) has a yellowish color and appears turbid (Figs. 3a and 3b). Microprobe analyses give up to 32 wt% Ce_2O_3, 15 wt% La_2O_3, 11 wt% Nd_2O_3 and smaller contents of the remaining REE (Table 9). REE patterns show LREE enrichment relative to the HREE with a positive Eu anomaly (Fig. 4g).

DISCUSSION

Peralkaline granitic rocks are commonly associated with subeconomic deposits of rare metals (Schmitt et al. 2002). The high valence and large ionic radius make REE incompatible with respect to common minerals in igneous systems and as a result, they remain in solution until the last stages of magmatic evolution, concentrating in residual melts that form pegmatites and

277 alkali granites (Krauskopf and Bird 1995). The difference in ionic radii between LREE and
278 HREE makes the former even more incompatible than the latter, explaining the enrichment of
279 highly fractionated granitic rocks in LREE. High field strength elements do not really substitute
280 in common minerals either due to their high charge, fairly large ionic radius and low initial
281 concentration (Krauskopf and Bird 1993). Elements like Zr, Ti and REE show a more compatible
282 behavior in common granitic melts, but in alkaline melts, they tend to concentrate in late
283 magmatic stages due to the presence of fluorine (Keppler 1993). Fractionation can segregate and
284 concentrate them in residual melts, where they form their own minerals like zircon, monazite,
285 allanite and titanite, if their concentrations are high enough.

286 **Stability conditions and origin of the minerals present**

287 The composition of the analyzed allanite-(Ce) (Table 2) is characteristic of magmatic
288 crystallization (Meintzer and Mitchell 1988). Secondary overgrowths and anhedral crystals with
289 lower LREE contents are REE-rich epidote. During post-magmatic alteration, LREE mobility
290 may result in the formation of REE-rich epidote after the breakdown of allanite (Rolland et al.
291 2003). Therefore, we consider the REE-rich epidotes of post-magmatic origin.

292 The REE titanosilicate chevkinite-(Ce) is the dimorph of perrierite-(Ce). It is stable in
293 water-rich melts at high temperatures (600-1000°C at 1-4 kbar), under oxygen fugacities ranging
294 from below the fayalite-quartz-magnetite buffer to higher than the Ni-NiO (Macdonald et al.
295 2002). The magmatic origin of chevkinite-(Ce) in the Wentworth granite is inferred from its
296 occurrence as inclusions in ferro-edenite (Figs. 5c and 5d), which has been interpreted as a
297 magmatic phase by Pe-Piper (2007), and from the interlocking texture between these two
298 minerals (Figs. 5e and 5f). Scaillet and Macdonald (2001) reported that the stability field of
299 chevkinite-(Ce) expands at high temperatures and oxidizing conditions. In peralkaline granites, it

probably crystallizes under conditions close to water saturation (Vlach and Gualda 2007). Chevkinite-(Ce) crystallizes at higher temperatures than allanite-(Ce) and was not found in any of the early HLBL granites (Table 1), indicating that the thermal effect of the later-emplaced gabbro intrusion was crucial for the crystallization of this mineral in the late granites.

Jiang (2006) suggested that chevkinite-(Ce) can be replaced by allanite-(Ce) and ilmenite during hydrothermal alteration. The Fe-Ti- rich (Table 3), yellow alteration halo observed around many of the chevkinite-(Ce) grains (Figs. 5a and 5b) in the Wentworth granite samples is interpreted as an early stage of chevkinite-(Ce) breakdown. The altered chevkinite-(Ce) in sample 6490 provides evidence of enrichment in Ti and depletion in Ca during hydrothermal alteration. This Ti enrichment is associated with the widest fractures, interpreted as a result of volume change during alteration. Loss of Ce presumably occurred earlier, as it affected the entire grain and not just the Ti-rich core (Fig. 6).

Small euhedral crystals of hingganite-(Y) occur adjacent to a larger anhedral crystal of secondary REE-rich epidote (Figs. 8c and 8d). This mode of occurrence suggests that the hingganite-(Y) predates the epidote and therefore is late magmatic. Magmatic enrichment in Y and chemically similar HREE could be expected to arise from fractionation of allanite-(Ce) and chevkinite-(Ce), which serve as LREE sinks.

Samarskite-(Y) occurs as small euhedral crystals (Figs. 9b and 9c), one of which contains an inclusion of euhedral zircon, and is therefore interpreted as late magmatic. This mineral was identified as samarskite-(Y) rather than compositionally similar fergusonite-(Y) in the basis of Ercit's (2005) discrimination diagrams for Nb-Y-REE oxides. None of the Wentworth compositions plot within the fergusonite-(Y) field (Fig. 12).

Fersmite differs from samarskite-(Y) in its low Y content and the predominance of LREE (Table 8). Both minerals are found as independent grains, but where they coexist, the samarskite-(Y) appears to have partially altered to fersmite, as indicated by the textural evidence; i.e. most samarskite-(Y) grains are enclosed by fersmite and fersmite appears in more corroded and fractured parts of the grain, where hydrothermal alteration would have been more intense (Figs. 9d and 9e).

The close association of titanite, TiO_2 and aeschynite-(Y) in one of the studied samples (Fig. 11) provides an opportunity for the study of Ti behavior in granitic systems. Their mode of occurrence suggests that Ti was mobilized at least locally, to form different mineral phases. From textural evidence alone, it is difficult to determine the paragenetic sequence between titanite and the TiO_2 mineral; however, the fact that they are hosted in alkaline, Ca-poor igneous rocks, allows us to make some assumptions. Clark and Williams-Jones (2004) stated that titanite can replace rutile only in rocks with Ca-rich bulk compositions and a high carbonate content, which does not apply to the Wentworth A-type granites due to their overall low Ca content. On the other hand, Tilley and Eggleton (2005) described complete breakdown of titanite to anatase due to hydrothermal alteration. Reaction of titanite with a mineralizing fluid to produce TiO_2 minerals was described by Abraham and Spooner (1995) in shear-zone-related igneous rocks. Therefore, we interpret the TiO_2 mineral in our sample as a product of titanite alteration.

The relationship between titanite and aeschynite-(Y) is more complex. The association of titanite with Y-REE-Ti oxides appears to be extremely rare (Liferovich and Mitchell 2005). In the Wentworth samples, aeschynite-(Y) occurs only in proximity to and in places closing polycrystalline titanite (Fig. 11). This relationship implies that aeschynite-(Y) post-dates titanite. Breakdown of titanite to TiO_2 indicates release of Ca and Si, but relatively low mobility of Ti at

this stage. Reaction of the residual Ti with a REE- and Y-bearing hydrothermal fluid could produce aeschynite-(Y). Textural evidence from the grain of altered chevkinite (Fig. 6) also indicates that REE were mobilized prior to Ti, as discussed earlier. Thus, we suggest that the formation of aeschynite-(Y), which requires REE mobility, occurred prior to the replacement of titanite by TiO_2, which would require increased Ti mobility.

The alteration of allanite-(Ce) to hydroxylbastnäsite-(Ce) (Figs. 3a and 3b) and the presence of fluorite suggest that the late evolution of the Wentworth granites involved their interaction with F-rich fluids. Furthermore the presence of secondary REE-rich epidote (Table 2) indicates removal of LREE from the primary host during alteration (Rolland et al., 2003). The mobility of REE is affected by HCO_3^- and SO_4^{2-} concentrations in the fluids. Even though the presence of hydroxylbastnäsite-(Ce) indicates the presence of CO_2 in the hydrothermal fluid, the relative importance of CO_2 to REE mobility in the Wentworth pluton is uncertain. The analyzed grain has low La/Nd ratios (1.3 to 1.4, Table 9); such low ratios are typically observed in low-CO_2 fluids (Rolland et al. 2003). It is therefore more likely that SO_4^{2-} anions were responsible for REE complexing and transport at that stage. The presence of abundant pyrite in the Folly Lake gabbro (Hilton 1998) and Byers Brook Formation (Piper et al. 1999) indicates that sulfate could be derived from oxidation of pyrite and released into the hydrothermal system facilitating REE mobility.

Zirconium is generally considered an immobile element and is highly stable in nonmagmatic environments; however, it can be mobile under hydrothermal conditions and high-pressure metamorphism (Tomaschek et al. 2003; Rubatto et al. 2008). High F concentrations can also promote Zr mobility (Rubin et al. 1993). An indication of Zr mobility in the Wentworth granites is the distinct optical and compositional zoning of the zircons in sample 6518 (Figs. 7c-

e). The rims of these zircons have less Zr than the core (Table 4) and appear porous and fractured. These overgrowths record Zr mobility in the presence of a F-rich fluid. Furthermore, the enrichment in Th in the fractured rims of these zircon crystals is interpreted as a result of hydrothermal alteration and, together with the presence of thorite-inclusions, observed in fractured magmatic zircons (Figs. 7a and 7b), implies the presence of Th in the fluids.

Relationship of REE minerals to host-rock chemistry

Chevkinite-(Ce) is interpreted to occur in rocks produced from evolved peralkaline magmas (Troll et al. 2003; Vlach and Gualda 2007). In contrast, allanite-(Ce) is the typical phase of metaluminous and peraluminous granites (Vlach and Gualda 2007). The Shand's index of all samples from the Wentworth pluton that contain chevkinite-(Ce) ranges between 1.00 and 1.10, very similar to that of the allanite-bearing samples, ranging between 1.00 and 1.16 (Table 1). All of the samples containing either chevkinite-(Ce) or allanite-(Ce) plot in the lower part of the metaluminous field, close to peralkaline field, with no significant variation. This indicates that the alkalinity of the parent magma was not the major factor that determined which of these two minerals was crystallized. Magmatic allanite-(Ce) and chevkinite-(Ce) are not known to coexist (Vlach and Gualda 2007), and this general rule applies to the Wentworth granite.

Fluorine abundance

Fluorine abundance appears to be an important factor in the formation of rare-metal minerals. Uher et al. (2009) related the presence of REE- and Nb-rich minerals like hingganite and samarskite to the presence of late-stage, F-rich fluids. The separation between HREE and LREE depends on their affinity to form complexes with F (Gramaccioli et al. 1999; Aurisicchio et al. 2001). Fluorine complexes of HREE are more stable compared to LREE complexes, which can be mobilized by SO_4^{2-}-rich fluids (Rolland et al. 2003). According to Aurisicchio et al.

(2001), as the activity of Y and HREE decreases, the LREE precipitate from the fluid to form LREE-enriched, late minerals (Fig. 13).

The presence of F-rich fluids is also suggested by the compositional characteristics of amphiboles from the Wentworth pluton (Pe-Piper 2007). Magmatic amphiboles from the early HLBL granites differ from those from the late granites only in having a higher F content. Breakdown of magmatic amphiboles can lead to the release of F as a volatile phase (Schönenberger et al. 2006). The lack of fluorine in the magmatic amphiboles from the late granites suggests that the anatectic process resulted in loss of incompatible F to hydrothermal circulation, so that it was less concentrated in the magmas that produced the syn- and post-gabbro granites (Fig. 13). These late F-rich fluids are presumably related to the mobilization of rare metals and HREE and the precipitation of fluorite.

The high level of F in the early magmatic amphiboles (Pe-Piper 2007) also indicate this element was in enriched in the parental magma. Fluorine increases the solubility of zircon, monazite and xenotime in granitic systems (Keppler 1993). Zircon is the major sink for rare metals like Th facilitating their retention in the melt until the late stages of magma evolution.

Relationship to pluton evolution

The evolutionary history of the minerals described above, started with the crystallization of the early HLBL granite of the Wentworth pluton. This was followed a few million years later by partial melting, which led to the anatexis of some of the early granite by the Folly Lake gabbro intrusion (Fig. 14). During the crystallization of the syn- and post-gabbro granites, the availability of heat from the gabbroic magma resulted in the crystallization of chevkinite-(Ce) rather than allanite-(Ce). Partial melting of the early granites resulted in the syn- and post-gabbro granitic melt depleted in F, Nb, Th and Rb (Koukouvelas et al. 2002; Pe-Piper 2007). These

differences suggest that during the partial melting, some volatiles were released to form a hydrothermal system that was able to transport certain incompatible elements (Fig. 14). These volatiles included fluorine released from the breakdown of amphibole, and sulfur from the decomposition of pyrite. Their release may have resulted from reheating of the crystallized early granite, which was not sufficient to cause anatexis.

The observation that HREE-rich minerals such as samarskite-(Y) are altered to LREE-rich minerals (Figs. 9d and 9e) suggests preferential F-complexing of HREE, promoting crystallization of HREE minerals, and leading to retention of the less-compatible LREE (probably as sulfate complexes) in the hydrothermal fluids (Fig. 14). It is likely these S-rich fluids that removed LREE from chevkinite (Fig. 6). Resetting of mica ages along the Rockland Brook Fault persisted for about 15 million years after the last major gabbro intrusion (Pe-Piper et al. 2004), suggesting that the observed sequence of mineral alteration could have occurred over a period of tens of millions of years (Fig. 14).

The evidence for hydrothermal alteration within the pluton cannot be precisely correlated with the dated phases of hydrothermal circulation. Nevertheless, some tentative interpretations can be made. Only the 320–315 Ma hydrothermal event in the Cobequid Shear Zone appears associated with significant carbonates (e.g., siderite and ankerite deposits at Londonderry, immediately south of the Folly Lake gabbro: Wright 1975). Thus, alteration of aeschynite-(Y) and titanite to TiO_2 could occur during the same event, when the amount of CO_2 in the fluid was sufficient to promote Ti mobility. Evidence from the carbonate hydroxylbastnäsite-(Ce) is ambiguous. The presence of carbonate implies high HCO_3^-, but the La/Nd ratios indicate low HCO_3^- , suggesting that the formation of this mineral was not necessarily related to any late

436 hydrothermal overprint, but possibly to an earlier hydrothermal system linked to the granite
437 emplacement.

438 The major characteristics of many REE-rare metal systems are their association with
439 alkaline magmatism and metasomatism, the presence of sodic amphibole and close or direct
440 association with carbonate and metasedimentary rocks. Only a few reported systems involve the
441 effects of more than one intrusive phase. In the Bergslagen mining region in Sweden, the
442 mineralization is restricted to marbles and felsic metavolcanic rocks that have been intruded by
443 at least two generations of plutonic rocks and hydrothermally altered (Holtstam and Andersson
444 2007). Similarities with the Wentworth pluton are the occurrence of sulfide mineralization and
445 the association of REE with F-rich minerals. The Amis complex in Namibia is another example
446 of a mineralized, late phase that intruded older anorogenic granites (Schmitt et al. 2002). As the
447 mineralization is hosted only in that late phase, the relationship between the development of the
448 mineralizing system and the evolution of the Amis anorogenic granites is not clear. At
449 Wentworth, on the other hand, rare-metal minerals are hosted by the granites of both the older
450 and younger phases and produced by a combination of anatexis (principally silicate minerals)
451 and later hydrothermal processes (mostly oxide minerals). To our knowledge, this type of
452 granite-hosted rare-metal mineralization has no analogues in the literature.

453 **CONCLUDING REMARKS**

454 The present work shows the variety of rare-metal accessory minerals in the Wentworth granite,
455 formed in several stages during the evolution of the pluton. The presence of F in the parental
456 magma facilitated the retention in the melt of such rare metals as Zr, Y, Th and Nb. Furthermore,
457 the presence of F affected the behavior of REE so that monazite-xenotime saturation was not
458 achieved and instead, allanite-(Ce) formed in the early Wentworth granite. Heat supplied by the

Wentworth gabbro led to the formation of chevkinite-(Ce) in the syn- and post-gabbro granites. Fractionation of allanite-(Ce) and chevkinite-(Ce) led to magma enrichment in middle and heavy rare earths, leading to the crystallization of hingganite-(Y) during the late magmatic stages. Remelting of the early granite caused F and S release due to the breakdown of amphibole and pyrite. These volatile components were incorporated in hydrothermal fluids that may have circulated for at least 15 Ma. Yttrium and middle to heavy REE, mobilized by F-complexing, were the first rare metals to precipitate from these fluids, forming samarskite-(Y) in late to post-magmatic stages. This caused relative LREE enrichment in the fluid that was enhanced by the presence of sulfur. Post-magmatic precipitation of LREE accounts for REE-rich epidote, fersmite and probably, hydroxylbastnäsite-(Ce). Carbonate and S-rich fluids were involved in regional hydrothermal circulation along the Cobequid-Chedabucto fault at 320-315 Ma. These fluids may have been responsible for late-stage Ti and REE mobilization. Alteration of aeschynite-(Y) and titanite to TiO_2 could be related to this late event. Correlation between mineral formation and the evolution of the Wentworth pluton provide a record of a unique mineralizing system affected by anatectic processes and evolving from primarily magmatic parageneses to hydrothermal ones.

Acknowledgements

The authors are grateful to Dr. David Piper for his invaluable help during fieldwork and for his significant contribution in improving the clarity of this work. We thank Associate Editor Dr. Anton Chakhmouradian for his thorough and constructive reviews. Sincere thanks to Dr. Pavel Uher, Dr. Milan Novák, Dr. Tania Martins and an anonymous reviewer for their comments and suggestions that greatly improved the manuscript. Dr. Filippo Ridolfi's assistance in the understanding of the chemistry of fluorocarbonates is greatly appreciated. We also thank Dan MacDonald for his help and support during microprobe analyses at the Regional Electron

Microprobe Centre at Dalhousie University and Drs. Victor Owen and Trevor MacHattie for the informative discussions and comments. Part of our analytical work was performed at the Regional Analytical Centre at Saint Mary's University. This project was supported by Natural Sciences and Engineering Research Council (NSERC) grants to Dr. Georgia Pe-Piper.

REFERENCES

Abraham, A.P.G. and Spooner, E.T.C. (1995) Late Archean regional deformation and structural controls on gold-quartz vein mineralization in the northwestern Slave Province, N.W.T., Canada. Canadian Journal of Earth Sciences, 32, 1132-1154.

Armbruster, T., Bonazzi, P., Akasaka, M., Bermanec, V., Chopin, C., Gieré, R., Heuss-Assbichler, S., Liebscher, A., Menchetti, S., Pan, Y., and Pasero M. (2006) Recommended nomenclature of epidote-group minerals. European Journal of Mineralogy, 28, 551-567.

Aurisicchio, C., De Vito, C., Ferrini, V., and Orlandi P. (2001) Nb-Ta oxide minerals from miarolitic pegmatites of the Baveno pink granite, NW Italy. Mineralogical Magazine, 65, 509-522.

Bhargava, S.K., Garg, A., and Subasinghe N.D. (2009) In situ high-temperature phase transformation studies of pyrite. Fuel, 88, 988-993.

Calder, J. H. (1998) The Carboniferous evolution of Nova Scotia. Geological Society of London, Special Publication, 143, 261-302.

Clark, J.R. and Williams-Jones, A.E. (2004) Rutile as a potential indicator mineral for metamorphosed metallic ore deposits. Diversification of Mineral Exploration of Quebec, final report, project SC2, pp 17.

504 Dessureau, G., Piper, D.J.W., and Pe-Piper, G. (2000) Geochemical evolution of earliest
505 Carboniferous continental tholeitic basalts along a crustal-scale shear zone:
506 southwestern Maritimes Basin, eastern Canada. Lithos, 50, 27-50.
507 Dunning, G.R., Barr, S.M., Giles, P.S., McGregor, D.C., Pe-Piper, G., and Piper D.J.W. (2002)
508 Chronology of Devonian to early Carboniferous rifting and igneous activity in
509 southern Magdalen Basin based on U-Pb (zircon) dating. Canadian Journal of Earth
510 Sciences, 39, 1219-1237.
511 Doig, R., Murphy, J.B., Pe-Piper, G., and Piper, D.J.W. (1996) U-Pb geochronology of the late
512 Paleozoic plutons, Cobequid Highlands, Nova Scotia, Canada: Evidence for late
513 Devonian emplacement adjacent to the Meguma-Avalon terrane boundary in the
514 Canadian Appalachians. Geological Journal, 31, 179-188.
515 Drake, M.J. and Weill, D.F. (1972) New rare earth elements standards for electron microprobe
516 analysis. Chemical Geology, 10, 179-181.
517 Ercit, T.S. (2005) Identification and alteration trends of granitic-pegmatite-hosted
518 (Y,REE,U,Th)-(Nb,Ta,Ti) oxide minerals: a statistical approach. Canadian
519 Mineralogist, 43, 1291-1303.
520 Ewing, R.C. (1975) The crystal chemistry of complex niobium and tantalum oxides. IV. The
521 metamict state: discussion. American Mineralogist, 60, 728-733.
522 Förster, H.J. (2000) Cerite-(Ce) and thorian synchysite-(Ce) from the Niederbobritzsch granite,
523 Erzgebirge, Germany: Implications for the differential mobility of the LREE and Th
524 during alteration. Canadian Mineralogist, 38, 67-79.
525 Frost, B.R., Barnes, C.G., Collins, W.J., Argulus, R.J., Ellis, D.J., and Frost, C.D. (2001) A
526 geochemical classification for granitic rocks. Journal of Petrology, 42, 2033-2048.

Gramaccioli, C.M., Diella, V., and Demartin, F. (1999) The role of fluoride complexes in REE geochemistry and the importance of 4*f* electrons: some examples in minerals. European Journal of Mineralogy, 11, 983-992.

Gower, D.P. (1988) Geology and Genesis of Uranium Mineralization in Subaerial Felsic Volcanic Rocks of The Byers Brook Formation and the Comagmatic Hart Lake Granite, Wentworth Area, Cobequid Highlands, Nova Scotia. MSc. Thesis, Memorial University of Newfoundland.

Hilton, E. (1998) Geochemistry and Chemical Mineralogy of Mafic Rocks of the Wentworth Plutonic Complex, Cobequid Highlands, Nova Scotia. BSc. Thesis, Saint Mary's University.

Holtstam, D. and Andersson, U.B. (2007) The REE minerals of the Bastnäs-type deposits, south-central Sweden. Canadian Mineralogist, 45, 1073-1114.

Jiang, N. (2006) Hydrothermal alteration of chevkinite-(Ce) in the Shuiquangou syenitic intrusion, northern China. Chemical Geology, 227, 100-112.

Keppler, H. (1993) Influence of fluorine on the enrichment of high field strength trace elements in granitic rocks. Contributions to Mineralogy and Petrology, 114, 479-488.

Krauskopf, K.B. and Bird, D.K. (1995) Introduction to Geochemistry, 3rd edn. McGraw-Hill, Boston, p. 647.

Koukouvelas, I., Pe-Piper, G., and Piper, D.J.W. (2002) The role of dextral transpressional faulting in the evolution of an early Carboniferous mafic-felsic plutonic and volcanic complex: Cobequid Highlands, Nova Scotia, Canada. Tectonophysics, 348, 219-246.

549 Liferovich, R.P. and Mitchell, R.H. (2005) Composition and paragenesis of Na-, Nb- and Zr-
550 bearing titanite from Khibina, Russia and crystal-structure data from synthetic
551 analogues. Canadian Mineralogist, 43, 795-812.
552 Macdonald, R. and Belkin, H. E. (2002) Compositional variation in minerals of the chevkinite-
553 group. Mineralogical Magazine, 66, 1075-1098.
554 Macdonald, R., Marshall, A.S., Dawson, J.B., Hinton, R.W., and Hill, P.G. (2002) Chevkinite-
555 group minerals from salic volcanic rocks of the East African Rift. Mineralogical
556 Magazine, 66, 287–299.
557 MacHattie, T.G. (2009) Magmatism, alteration and polymetallic mineralization in late Devonian
558 to early Carboniferous felsic volcanic and plutonic rocks of the eastern Cobequid
559 Highlands. Nova Scotia Department of Natural Resources, Mineral Resources
560 Branch, Report of Activities, p. 65-75.
561 Maniar, P.D. and Piccoli, P.M. (1989) Tectonic discrimination of granitoids. Geological Society
562 of America Bulletin, 101, 635-643.
563 Meintzer, R.E. and Mitchell, R.S. (1988) The epigene alteration of allanite. Canadian
564 Mineralogist, 26, 945-955.
565 Miller, B.V., Nance, R.D., and Murphy, J.B. (1995) Kinematics of the Rockland Brook fault,
566 Nova Scotia: implications for the interaction of the Meguma and Avalon terranes,
567 Journal of Geodynamics, 19, 253-270.
568 Murphy, J.B., Waldron, J.W.F., Kontak, D.J., Pe-Piper, G., and Piper, D.J.W. (2011) Minas Fault
569 Zone: Late Paleozoic history of an intra-continental orogenic transform fault in the
570 Canadian Appalachians. Journal of Structural Geology, 33, 312-328.

Orris, G. and Grauch, R.I. (2002) Rare earth element mines, deposits, and occurrences. U.S. Geological Survey, Open-file report 02-189.

Parnell, J. (2004) Titanium mobilization by hydrocarbon fluids related to sill intrusion in a sedimentary sequence, Scotland. Ore Geology Reviews, 24, 155-167.

Pe-Piper, G. (2007) Relationship of amphibole composition to host-rock geochemistry: the A-type gabbro-granite Wentworth pluton, Cobequid Shear Zone, eastern Canada. European Journal of Mineralogy, 19, 29-38.

Pe-Piper, G. and Piper, D.J.W. (2002) A synopsis of the geology of the Cobequid Highlands, Nova Scotia. Atlantic Geology, 38,145-160.

Pe-Piper, G. and Piper, D.J.W. (2005) Bedrock Geological Map of the Wentworth Area (parts of NTS sheets 11E/05, 11E/06, 11E/11 and 11E/12), Cobequid Highlands, Nova Scotia, scale 1:50 000. Nova Scotia Department of Natural Resources, Mineral Resources Branch, open file map, OFM ME 2005-116.

Pe-Piper, G., Reynolds P.H, Nearing, J., and Piper, D.J.W. (2004) Early Carboniferous deformation and mineralization in the Cobequid Shear Zone, Nova Scotia: an $^{40}Ar/^{39}Ar$ geochronology study. Canadian Journal of Earth Sciences, 41, 1425-1436.

Piper, D.J.W., Dessureau, G., and Pe-Piper, G. (1999) Occurrence of early Carboniferous high-Zr rhyolites, Cobequid Highlands, Nova Scotia: Temperature effect of a contemporaneous mafic magma. Canadian Mineralogist, 37, 619-634.

Rabbia, O.M., Hernández, L.B., French, D.H., King, R.W., and Ayers, J.C. (2009) The El Teniente porphyry Cu-Mo deposit from a hydrothermal rutile perspective. Mineralium Deposita, 44, 849-866.

Ridolfi, F., Renzulli, A., Macdonald, R., and Upton, B.G.J. (2006) Peralkaline syenite autoliths from Kilombe volcano, Kenya Rift Valley: evidence for subvolcanic interaction with carbonatitic fluids. Lithos, 91, 373-392.

Rolland, Y., Cox, S., Boullier, A., Pennacchioni, G., and Mancktelow, N. (2003) Rare earth and trace element mobility in mid-crustal shear zones: insights from the Mont Blanc Massif (Western Alps). Earth and Planetary Science Letters, 214, 203-219.

Rubatto, D., Müntener, O., Barnhoorn, A., and Gregory, C. (2008) Dissolution-reprecipitation of zircon at low-temperature, high-pressure conditions (Lanzo Massif, Italy). American Mineralogist, 93, 1519-152.

Rubin, J. N., Henry, C. D., and Price, J. G. (1993) The mobility of zirconium and "immobile" elements during hydrothermal alteration. Chemical Geology, 110, 29-47.

Saveleva, V.B. and Karmanov, N.S. (2008) REE minerals of alkaline metasomatic rocks in the Main Sayan Fault. Geology of Ore Deposits, 50, 681-696.

Scaillet, B. and Macdonald, R. (2001) Phase relations of peralkaline silicic magmas and petrogenetic implications. Journal of Petrology, 42, 825-845.

Schmitt, A.K., Trumbull, R.B., Dulski, P., and Emmermann, R. (2002) Zr-Nb-REE mineralization in peralkaline granites from the Amis Complex, Brandberg (Namibia): Evidence for magmatic pre-enrichment from melt inclusions. Economic Geology, 97, 399-413.

Schönenberger, J., Marks, M., Wagner, T., and Markl, G. (2006) Fluid-rock interaction in autoliths of agpaitic nepheline syenites in the Ilímaussaq intrusion, South Greenland. Lithos, 91, 331-351.

615 Seifert, W., Rhede, D., Förster, H.-J., and Thomas, R. (2009) Accessory minerals as fingerprints
616 for the thermal history and geochronology of the Caledonian Rumburk granite.
617 Neues Jahrbuch für Mineralogie Abhandlungen, 186, 215-233
618 Škoda, R. and Novák, M. (2007) Y, REE, Nb, Ta, Ti-oxide (AB_2O_6) minerals from REL-REE
619 euxenite-subtype pegmatites of the Třebíč Pluton, Czech Republic; substitutions
620 and fractionation trends. Lithos, 95, 43-57.
621 Tilley, D.B. and Eggleton, R.A. (2005) Titanite low-temperature alteration and Ti mobility.
622 Clays and Clay Minerals, 53, 100-107.
623 Tomaschek, F., Kennedy, A.K., Villa, I.M., Lagos, M., and Ballhaus, C. (2003) Zircons from
624 Syros, Cyclades, Greece-Recrystallization and mobilization of zircon during high-
625 pressure metamorphism. Journal of Petrology, 44, 1977-2003.
626 Troll, V.R., Sachs, P.M., Schmincke, H.U., and Sumita, M. (2003) The REE-Ti mineral
627 chevkinite in comenditic magmas from Gran Canaria, Spain: a SYXRF-probe
628 study. Contributions to Mineralogy and Petrology, 145, 730–741.
629 Uher, P., Ondrejka, M., and Konečný, P. (2009) Magmatic and post-magmatic YREE-Th
630 phosphate, silicate and Nb-Ta-Y-REE oxide minerals in A-type metagranite: an
631 example from the Turčok massif, western Carpathians, Slovakia. Mineralogical
632 Magazine, 73, 1009-1025.
633 Vlach, S.R.F. and Gualda, G.A.R. (2007) Allanite and chevkinite in A-type granites and syenites
634 of the Graciosa Province, southern Brazil. Lithos, 97, 98-121.
635 Wang, R.C., Wang, D.Z., Zhao, G.T., Lu, J.J., Chen, X.M., and Xu, S.J. (2001) Accessory
636 mineral record of magma-fluid interaction in the Laoshan I- and A-type granitic
637 complex, eastern China. Physics and Chemistry of the Earth, 26, 835-849.

Whitney, D.L. and Evans, B.W. (2010) Abbreviations for names of rock-forming minerals. American Mineralogist, 95, 185-187.

Wood, S.A. and Ricketts, A. (2000) Allanite-(Ce) from the Eocene Casto granite, Idaho: Response to hydrothermal alteration. Canadian Mineralogist, 38, 81-100.

Wright, J.D. (1975) Iron deposits of Nova Scotia. Nova Scotia Department of Natural Resources, Economic Geology Series, 75 (1), 154p.

List of captions

Figure 1: (a) Regional location of Wentworth Pluton. (b) Geological map of the Wentworth pluton area showing the geographic distribution of the studied samples (modified from Koukouvelas et al. 2002). (c) Geochronological data from the studied formations combined with the stratigraphy of the associated volcanic rocks (Arf = arfvedsonite, Bt = biotite, Hbl = hornblende). Ages from Doig et al. (1996) and Pe-Piper et al. (2004), recalibrated as in Murphy et al. (2011).

Figure 2: Compositional variation of the analyzed samples from the Wentworth pluton (fields after Maniar and Piccoli 1989). Open symbols represent probable samples of the mentioned types. Sample numbers in italics are allanite-bearing samples. Underlined numbers indicate chevkinite-bearing samples.

Figure 3: Microphotographs (a and c) and BSE images (b and d) of allanite-(Ce) (Aln). Images (a) and (b) show euhedral magmatic allanite-(Ce) replaced by hydroxylbastnäsite-(Ce) (H-bas) from sample 7658. Images (c) and (d) show inclusions of magmatic allanite-(Ce) in an amphibole crystal (Amp) surrounded by quartz (Qz) and feldspar (Fsp).

Figure 4: Chondrite-normalized REE patterns for (a) allanite-(Ce), (b) chevkinite-(Ce), (c) hingganite-(Y), (d) samarskite-(Y), (e) fersmite, (f) aeschynite-(Y) and (g) hydroxylbastnäsite-(Ce).

Figure 5: Microphotographs (a, c and e) and BSE images (b, d and f) of chevkinite-(Ce) (Che) from sample 7710. Images (a) and (b) show a discrete grain, whereas images (c) and (d) show a chevkinite-(Ce) inclusion in amphibole.

Figure 6: X-ray compositional maps (a-e) and BSE image (f) of an altered (?) chevkinite-(Ce) (sample 6490). The crystal shows zoning involving variations in Ti and Ca (images c and d, respectively), whereas Fe shows a patchy distribution within the crystal.

Figure 7: Microphotographs (a, c and d) and BSE images (b and e) of magmatic zircon (Zrn). Figures (a) and (b) show zircon crystals from the HLBL granite (9832) containing Th-rich inclusions (bright areas in BSE image). Images (c- e) show zircon inclusions in feldspar (sample 6518). Zrn I represents a clear zircon core whereas Zrn II indicates a Th-rich zircon overgrowth (Rc Fsp = recrystallized contact between the two feldspar crystals, Fr = fractures). Numbers indicate spot analyses in Tables 4 and 6.

Figure 8: REE-rich epidote enclosing two hingganite crystals (Hing).

Figure 9: Image (a) is a BSE image of samarkite-Y grains associated with a thorite-like phase (Trt) from sample 6490. Images (b and d) are microphotographs and images (c and d) are BSE images of samarskite-Y (Sam-Y) and fersmite (Fers) grains. Images (b) and (c) are from sample 9827A. Images (d) and (e) are from sample 9831. Numbers indicate spot analyses listed in Table 7.

Figure 10: Microphotograph (a) and BSE image (b) of a Nb-oxide mineral that resembles fersmite occurring as an inclusion in fluorite (Fl) (sample 7658).

682 Figure 11: Microphotograph (a) and BSE image (b) of aeschynite-(Y) (Aes-Y) in a clot of
683 titanite (Tnt) crystals associated with TiO_2 mineral (Tna) in sample 9832 (analysis 237,
684 Table 8.
685 Figure 12: Plot of canonical variables CV1% vs. CV2% for Nb oxides from the Wentworth
686 granite, in a three-group model introduced by Ercit (2005). CV1 = 0.106Ca- 0.077Fe+
687 0.220Y+ 0.280LREE+ 0.137HREE+ 0.100U+ 0.304Ti+ 0.097Nb+ 0.109Ta- 12.81.
688 CV2= -0.013Ca- 0.371Fe- 0.395Y- 0.280LREE- 0.265HREE- 0.182U- 0.085Ti-
689 0.166Nb- 0.146Ta+ 17.29.
690 Figure 13: Summary of the magmatic processes during the evolution of the Wentworth pluton
691 related to the formation of the studied minerals. Fed = ferro-edenite, Fwn =
692 ferrowinchite, Ktp = Katophorite, Arf = arfvedsonite, Tnt = titanite, Trt = thorite, Ep =
693 epidote, Aln = allanite (abbreviations as in Whitney and Evans, 2010). Sam-Y =
694 samarskite-(Y), Hing = hingganite-(Y), Che = chevkinite, Fers = fersmite, H-bas =
695 hydroxylbastnäsite (abbreviations as in Orris and Grauch, 2002). Aes-Y = aeschynite-Y,
696 Tna = TiO_2 mineral.
697 Figure 14: Summary of the geological evolution of the Wentworth pluton combined with the
698 paragenetic sequence of the rare-metal accessory minerals described in the present work.
699 Geological evolution synthesized from Pe-Piper and Piper (2002), Koukouvelas et al.
700 (2002), Pe-Piper et al. (2004) and Murphy et al. (2011).

Table 1: Petrology and geochemistry of the studied samples from the Wentworth pluton.

Sample	Type (Based on relative age)	Mineral association	ANK	Fe-index	Minerals analyzed
4636	HLBL granite, definite	Qz,Pl,Kfs, Amp (s,s-c),Zrn, qz (sec), clay minerals (sec), REE-ep, Ilm, Mag.	1.16	0.75	Allanite-(Ce), ilmenite, titanian magnetite, titaniferous magnetite, fersmite
9831	HLBL granite, probable	Qz,Pl,Kfs, Bt, Amp (s,s-c),Zrn, Opq, Ap, Aln, Sam-Y, Fers, Qz(sec), mica (sec), clay minerals (sec)	1.04	0.98	Allanite, samarskite, fersmite
9832	HLBL granite, probable	Qz,Pl,Kfs, Bt, Amp (s,s-c),Zrn, Opq, Ap, Aln, Aes-Y, Sam-Y, Fers, Tna, Qz(sec), mica (sec), clay minerals (sec)	1.06	0.95	Allanite-(Ce), zircon, aeschynite-(Y), samarskite-(Y), fersmite, TiO_2 mineral
7658	Granite intruding the Byers Brook Fm., definite	Qz,Pl,Kfs, Bt, Amp (s,s-c),Zrn, Opq, Ap, Qz(sec), Aln, Aes-Y, H-Bas, mica (sec), clay minerals (sec)	0.98	0.91	Allanite-(Ce), fersmite, hydroxylbastnäsite-(Ce)
5056	Syn-gabbro granite definite	Qz,Pl,Kfs, Bt, Amp (c),Zrn, Ilm, Mag, Ap, Qz(sec), mica (sec), clay minerals (sec)	0.84	0.83	Ilmenite, titaniferous magnetite, magnetite
6490	Syn-gabbro granite definite	Qz,Pl,Kfs, Amp (s,s-c),Zrn, Che, Mag, Qz (sec), clay minerals (sec)	1.04	0.97	Chevkinite-(Ce), thorite, titaniferous magnetite, magnetite, samarskite-(Y)
6419	Large post-gabbro bodies of granite, probable	Qz,Pl,Kfs, Amp (s),Zrn,Che, REE-ep, Hing, Opq, mica (sec)	1.11	0.99	Chevkinite-(Ce), allanite-(Ce), zircon, hingganite-(Y)
6518	Large post-gabbro bodies of granite, probable	Qz,Pl,Kfs, Amp (s,s-c),Zrn, Che, Ilm, Mag, Bt (sec), Chl (sec)	1.14	0.99	Chevkinite-(Ce), zircon, ilmenite, magnetite
7710	Late fine grained granite dyke , definite	Qz,Pl,Kfs, Amp (s,s-c), Che, Zrn, Ilm, Mag, Ep (sec)	1.08	0.96	Chevkinite-(Ce), ilmenite, titanian magnetite, titaniferous magnetite
9827 a	Late fine grained granite dyke , definite	Qz,Pl,Kfs, Bt, Amp (s,s-c),Zrn, Opq, Ap, Qz(sec), Aln, Sam-Y, mica (sec), clay minerals (sec)	0.94	0.9	Allanite-(Ce), samarskite-(Y)
9827b	Late fine grained granite dyke , definite	Qz,Pl,Kfs, Bt, Amp (s,s-c),Zrn, Mag, Ap, Qz(sec), mica (sec), clay minerals (sec), Hem.	1.02	0.92	Magnetite, hematite

Notes:
1) ANK= Shand's index $[Al_2O_3/(Na_2O+K_2O)]$, used as in Maniar and Piccoli, (1989); 2) Fe-index = FeOt/ (FeOt+MgO,) after Frost et al. (2001); 3) Mineral abbreviations (after Whitney and Evans 2010): Qz = quartz, Pl = plagioclase, Kfs = K-feldspar, Bt = biotite, Amp = amphibole, Zrn = zircon, Opq = opaque minerals, Ap = apatite, Chl = chlorite, Ep = epidote, Hem = hematite, Mag = magnetite, Ilm = ilmenite. Aln = allanite, Che = chevkinite, Aes-Y = aeschynite-Y, Sam-Y - samarskite-Y, Hing = hingganite, H-bas = hydroxylbastnäsite, (sec) = secondary mineral, (s) = sodic, (s-c) = sodic-calcic, (c) = calcic.

Conditions and standards used for microprobe analyses.

Element measured	Line	Peak Position	Standard	Crystal	Detection limit (wt%)	Correction Factors (peak overlap correction)
P	Kα	197.327	Monazite	PETJ	0.02	
Nb	Lα	183.487	Columbite	PETJ	0.05	
Ta	Lα	106.200	Tantalite	LIFH	0.07	
Si	Kα	77.531	Sanidine	TAP	0.01	
Ti	Kα	88.207	Kaersutite	PETJ	0.03	Ti-Hf 0.05429
Th	Mα	132.606	ThO_2_MAX	PETJ	0.04	
U	Mβ	119.104	UO_2	PETJ	0.04	
Zr	Lα	194.590	Zirconia	PETJ	0.04	Zr-P 0.00110
Hf	Lα	109.527	Zirconia	LIFH	0.14	Hf-Ho 0.05675 and Hf-Er 0.53361
Y	Lα	70.180	YAG	TAP	0.02	
Al	Lα	90.712	Sanidine	TAP	0.01	
La	Lα	185.485	$LaPO_4$_MAX	LIF	0.05	
Ce	Lα	178.226	$CePO_4$_MAX	LIF	0.04	
Pr	Lβ	157.292	REE3 (Drake and Weill, 1972)	LIFH	0.08	
Nd	Lβ	150.924	REE2 (Drake and Weill, 1972)	LIFH	0.08	
Sm	Lβ	139.251	REE2 (Drake and Weill, 1972)	LIFH	0.08	
Eu	Lα	147.767	REE1 (Drake and Weill, 1972)	LIFH	0.04	
Gd	Lβ	128.794	REE1 (Drake and Weill, 1972)	LIFH	0.12	
Dy	Lα	132.811	REE4 (Drake and Weill, 1972)	LIF	0.06	
Ho	Lα	128.629	REE4 (Drake and Weill, 1972)	LIFH	0.06	
Er	Lα	124.120	REE4 (Drake and Weill, 1972)	LIF	0.08	Er-Nb 0.08450 and Er-Hf 0.00263
Yb	Lα	116.276	REE2 (Drake and Weill, 1972)	LIF	0.08	
Fe	Kα	199.338	Magnetite53	LIF	0.02	
Mn	Kα	146.214	Pyrolusite	LIF	0.02	
Ca	Kα	107.711	F-apatite	PETJ	0.01	
F	Kα	199.338	F-apatite	TAPH	0.03	F-Ce 0.05096

Table 2: Representative electron-microprobe analyses and formulae of allanite-(Ce) and REE-rich epidote ($A_2M_3[T_2O_7][TO_4](O,F)(OH,O)$)

Sample	6419	6419	7658	9827A	9827A	9831	9832
Mineral	ep	ep	ep	aln	aln	aln	aln
Analysis	87	88	73	239	240	215	230
SiO_2	34.97	35.87	33.88	31.13	31.05	33.15	32.73
TiO_2	b.d	b.d	0.10	0.05	0.34	0.11	0.23
ThO_2	b.d	0.11	b.d	0.13	0.11	0.06	b.d
Al_2O_3	14.49	19.42	16.14	14.71	14.45	16.79	18.29
Y_2O_3	0.29	1.40	0.11	0.50	0.73	0.04	0.24
La_2O_3	2.88	2.24	3.25	5.16	4.44	4.68	5.26
Ce_2O_3	5.72	3.63	7.66	11.10	11.27	14.10	9.83
Pr_2O_3	0.53	0.41	0.88	1.18	1.26	1.09	0.95
Nd_2O_3	2.15	1.56	2.61	4.09	4.23	2.56	2.57
Sm_2O_3	0.43	0.33	0.35	0.64	0.82	0.13	0.22
Eu_2O_3	0.13	0.13	0.22	0.31	0.28	0.23	0.19
Gd_2O_3	0.25	0.52	0.12	0.48	0.59	b.d	0.11
Dy_2O_3	0.08	0.33	0.20	0.47	0.66	0.22	0.17
FeOt	18.16	14.39	16.48	15.93	14.81	14.31	12.20
MnO	0.07	0.12	0.34	0.77	1.19	0.42	0.42
CaO	15.77	16.77	14.33	10.15	10.26	10.81	12.67
Total	95.90	97.23	96.68	96.78	96.50	98.69	96.07
Norm.	**Si=3**	**Si=3**	**Si=3**	**Σ=8**	**Σ=8**	**Si=3**	**Si=3**
Si	3.000	3.000	3.000	3.029	3.036	3.000	3.000
Al	0.000	0.000	0.000	0.000	0.000	0.000	0.000
ΣT	**3.000**	**3.000**	**3.000**	**3.029**	**3.036**	**3.000**	**3.000**
Ti	0.000	0.000	0.007	0.004	0.025	0.007	0.016
Al	1.538	1.970	1.727	1.687	1.665	1.854	2.010
Fe	1.368	1.036	1.252	1.297	1.211	1.122	0.951
Mn	0.005	0.008	0.026	0.063	0.099	0.034	0.033
Σ M	**2.911**	**3.014**	**3.012**	**3.050**	**3.000**	**3.017**	**3.011**
Ca	1.522	1.546	1.394	1.058	1.075	1.085	1.265
La	0.096	0.071	0.109	0.185	0.160	0.162	0.181
Ce	0.189	0.114	0.255	0.396	0.403	0.484	0.336
Pr	0.017	0.013	0.029	0.042	0.045	0.037	0.032
Nd	0.069	0.048	0.085	0.142	0.148	0.086	0.085
Sm	0.013	0.010	0.011	0.021	0.028	0.004	0.007
Eu	0.004	0.004	0.007	0.010	0.009	0.007	0.006
Gd	0.007	0.015	0.004	0.015	0.019	0.001	0.003
Dy	0.002	0.009	0.006	0.015	0.021	0.007	0.005
Ho	0.000	0.002	0.000	0.000	0.003	0.000	0.000
Er	0.001	0.000	0.004	0.003	0.006	0.000	0.000
Yb	0.000	0.000	0.000	0.000	0.000	0.000	0.000
Th	0.001	0.002	0.000	0.003	0.002	0.001	0.000
U	0.000	0.000	0.002	0.000	0.000	0.001	0.000
Nb	0.002	0.000	0.000	0.002	0.001	0.000	0.004
Ta	0.000	0.000	0.000	0.000	0.000	0.001	0.000
Zr	0.000	0.000	0.000	0.000	0.000	0.000	0.000
Y	0.014	0.064	0.005	0.026	0.038	0.002	0.012
ΣREE	0.400	0.290	0.510	0.830	0.840	0.790	0.660
Σ A	**1.938**	**1.899**	**1.910**	**1.917**	**1.958**	**1.877**	**1.937**

Notes:
b.d= below detection limit. Elements calculated in the basis of 8 cations . When calculations yielded Si> 3.05 then it is normalized to Si-=3 (Armbruster et al. 2006).

Table 3: Representative electron-microprobe analyses and formulae of chevkinite-(Ce) ($A_4BC_2D_2Si4O_{22}$)

Sample	6518	6518	6518	6518	6518	7710	7710	7710
Analysis	71	72	74	80	82	70	89	122
P_2O_5	0.04	0.02	0.05	0.04	0.05	0.05	0.05	0.37
Nb_2O_5	0.75	0.80	0.78	0.79	0.55	2.16	0.97	3.10
SiO_2	20.06	19.97	20.43	20.37	20.32	19.82	20.38	18.26
TiO_2	19.15	18.72	18.30	18.66	18.62	16.88	18.09	19.89
ZrO_2	0.70	0.40	0.66	0.46	0.55	0.33	0.38	0.46
ThO_2	0.41	0.16	0.45	0.34	0.30	0.88	0.38	1.72
Al_2O_3	0.12	0.13	0.13	0.11	0.10	0.11	0.12	0.21
Y_2O_3	0.56	0.58	0.59	0.63	0.67	0.76	0.76	1.02
La_2O_3	10.69	10.90	10.67	10.69	10.81	10.90	10.32	10.20
Ce_2O_3	21.03	21.06	20.32	20.90	20.53	20.77	21.12	18.23
Pr_2O_3	1.95	1.74	1.87	1.85	1.92	1.85	2.10	1.67
Nd_2O_3	8.83	8.98	8.96	8.54	8.64	7.76	9.22	6.28
Sm_2O_3	1.20	1.00	0.92	0.94	0.88	0.90	1.24	0.82
Eu_2O_3	0.60	0.55	0.61	0.52	0.57	0.63	0.67	0.43
Gd_2O_3	0.57	0.54	0.72	0.73	0.46	0.57	0.70	0.61
Dy_2O_3	0.17	0.30	0.26	0.30	0.31	0.33	0.30	0.33
FeOt	11.07	11.61	10.88	10.79	10.86	11.62	11.58	11.98
MgO	b.d	0.04	0.05	0.02	0.01	0.08	0.07	b.d
CaO	2.78	2.61	2.61	2.69	2.64	2.56	2.43	3.16
F	b.d	b.d	b.d	b.d	b.d	b.d	b.d	b.d
Total	100.66	100.10	99.23	99.35	98.79	98.93	100.88	98.72
Y	0.060	0.064	0.065	0.069	0.073	0.084	0.083	0.111
Th	0.019	0.007	0.021	0.016	0.014	0.042	0.017	0.080
La	0.802	0.823	0.809	0.808	0.822	0.838	0.776	0.769
Ce	1.566	1.580	1.529	1.569	1.549	1.585	1.577	1.364
Pr	0.144	0.130	0.140	0.138	0.144	0.140	0.156	0.124
Nd	0.641	0.657	0.658	0.625	0.636	0.577	0.671	0.458
Sm	0.084	0.071	0.065	0.066	0.062	0.064	0.087	0.058
Eu	0.041	0.038	0.042	0.036	0.040	0.045	0.047	0.030
Gd	0.039	0.037	0.049	0.050	0.031	0.039	0.047	0.042
Dy	0.011	0.020	0.017	0.020	0.020	0.022	0.020	0.022
Ca	0.605	0.573	0.575	0.590	0.583	0.571	0.531	0.692
Sum A	**4.019**	**3.999**	**3.972**	**3.991**	**3.979**	**4.007**	**4.016**	**3.748**
Fe	1.000	1.000	1.000	1.000	1.000	1.000	1.000	1.000
Sum B	**1.000**	**1.000**	**1.000**	**1.000**	**1.000**	**1.000**	**1.000**	**1.000**
Fe	0.881	0.998	0.870	0.850	0.872	1.024	0.975	1.047
Mg	0.000	0.012	0.014	0.006	0.003	0.026	0.021	0.000
Ti	0.928	0.884	0.828	0.878	0.885	0.645	0.775	1.057
Al	0.029	0.030	0.031	0.025	0.025	0.027	0.028	0.050
Zr	0.070	0.040	0.066	0.046	0.055	0.034	0.038	0.045
Nb	0.069	0.074	0.073	0.074	0.052	0.204	0.090	0.286
Ta	0.000	0.000	0.000	0.000	0.000	0.000	0.000	0.000
Sum C	**1.976**	**2.038**	**1.881**	**1.879**	**1.892**	**1.959**	**1.926**	**2.485**
Ti (D)	2.000	2.000	2.000	2.000	2.000	2.000	2.000	2.000
Si	4.077	4.090	4.199	4.177	4.186	4.130	4.157	3.731
Σcations	**13.072**	**13.128**	**13.052**	**13.048**	**13.057**	**13.096**	**13.099**	**12.965**

Notes:
b.d= below detection limit. Analysis 122 represents a yellowish alteration halo around chevkinite. Formula

Table 4: Representative electron-microprobe analyses and formulae of zircon (ATO_4)

Sample	6419	6419	6518	6518	6518	9832
Analysis	120	121	154	155	157	197
P_2O_5	b.d	0.28	b.d	0.21	0.51	0.39
SiO_2	30.31	30.58	32.61	31.69	30.16	30.99
ZrO_2	67.34	63.88	63.74	59.40	54.79	60.47
HfO_2	0.81	1.24	0.85	0.92	2.52	1.66
ThO_2	0.00	0.13	b.d	0.44	4.01	1.22
UO_2	0.11	0.10	0.03	0.35	0.22	0.36
Y_2O_3	0.23	1.28	0.18	2.68	2.96	2.42
Gd_2O_3	0.22	0.10	b.d	0.08	0.17	0.35
Dy_2O_3	0.10	0.09	0.14	0.31	0.25	0.43
Er_2O_3	0.03	0.36	0.10	0.43	0.44	0.66
Yb_2O_3	0.04	0.32	0.13	0.37	0.48	0.96
FeOt	0.04	0.06	0.06	0.17	0.60	0.19
CaO	0.02	0.04	b.d	0.05	0.08	0.10
Total	99.25	98.45	97.85	97.09	97.18	100.21
P	0.000	0.007	0.000	0.006	0.014	0.010
Si	0.952	0.967	1.016	1.009	0.988	0.976
Total (T)	**0.952**	**0.974**	**1.016**	**1.014**	**1.002**	**0.986**
Zr	1.032	0.985	0.969	0.922	0.875	0.929
Hf	0.007	0.011	0.008	0.008	0.024	0.015
Th	0.000	0.001	0.000	0.003	0.030	0.009
U	0.001	0.001	0.000	0.003	0.002	0.003
Y	0.004	0.022	0.003	0.045	0.052	0.041
Gd	0.002	0.001	0.000	0.001	0.002	0.004
Dy	0.001	0.001	0.001	0.003	0.003	0.004
Er	0.000	0.004	0.001	0.004	0.005	0.007
Yb	0.000	0.003	0.001	0.004	0.005	0.009
Fe	0.001	0.002	0.002	0.005	0.017	0.005
Ca	0.000	0.001	0.000	0.002	0.003	0.003
Total (A)	**1.049**	**1.031**	**0.985**	**0.999**	**1.014**	**1.028**
Total	**2.001**	**2.005**	**2.001**	**2.013**	**2.016**	**2.014**

Notes:
1)b.d= below detection limit. Formula calculated in the basis of 4 oxygen atoms.

Table 5: Representative electron-microprobe analyses and formulae of hingganite-(Y) ($A_2Be_2T_2O_8(OH)_2$)

Sample	6419	6419	6419	6419
Analysis	86	143	145	146
SiO_2	26.38	25.98	24.61	25.03
Y_2O_3	26.43	31.30	18.22	18.29
La_2O_3	0.82	0.26	0.95	1.05
Ce_2O_3	4.40	1.77	7.56	7.84
Pr_2O_3	0.83	0.33	1.68	1.73
Nd_2O_3	5.50	3.37	10.36	10.77
Sm_2O_3	2.27	1.59	2.62	2.66
Eu_2O_3	0.31	0.14	0.68	0.72
Gd_2O_3	4.46	5.01	4.50	4.56
Dy_2O_3	4.56	5.04	3.83	3.83
Ho_2O_3	1.59	1.61	1.37	1.38
Er_2O_3	1.90	2.72	1.38	1.62
Yb_2O_3	1.04	1.42	0.35	0.35
FeOt	4.95	3.85	6.01	6.06
CaO	1.17	0.91	0.81	0.81
Total	86.61	85.30	84.93	86.70
Si	2.000	2.000	2.000	2.000
Sum T	**2.000**	**2.000**	**2.000**	**2.000**
Y	0.97	1.16	0.70	0.69
La	0.02	0.01	0.03	0.03
Ce	0.11	0.05	0.20	0.20
Pr	0.02	0.01	0.04	0.04
Nd	0.14	0.08	0.27	0.27
Sm	0.05	0.04	0.06	0.06
Eu	0.01	0.00	0.02	0.02
Gd	0.10	0.12	0.11	0.11
Dy	0.10	0.11	0.09	0.09
Ho	0.04	0.04	0.03	0.03
Er	0.04	0.06	0.03	0.04
Yb	0.02	0.03	0.01	0.01
Fe	0.29	0.23	0.36	0.36
Ca	0.09	0.07	0.06	0.06
Sum A	**2.000**	**2.000**	**2.000**	**2.000**

Notes:
1)b.d= below detection limit; 2) n.d.= not determined. Formula calculated on the basis of 10 oxygens, Si = 2 atoms, Ca+Fe+Y+REE=2 atoms, Be=2 atoms according to the theoretical formula of hingganite. However Be was not determined.

Table 6: Representative electron-microprobe analyses and formulae of thorite-like phase (ABO_4)

Sample	6490	9832	9832
Analysis	97	199	210
P_2O_5	4.47	0.22	0.71
Nb_2O_5	7.72	6.78	0.15
SiO_2	12.83	18.57	17.20
TiO_2	3.26	0.32	0.02
ZrO_2	n.d	11.31	1.39
HfO_2	n.d	0.47	0.29
ThO_2	49.43	40.53	58.67
UO_2	0.76	1.41	3.53
Al_2O_3	1.02	0.33	0.15
Y_2O_3	2.12	2.93	1.64
La_2O_3	0.12	0.07	0.13
Ce_2O_3	0.37	0.27	0.20
Nd_2O_3	0.45	0.18	b.d
Gd_2O_3	0.33	0.17	0.46
Dy_2O_3	0.49	0.39	0.52
Ho_2O_3	0.10	0.17	0.18
Er_2O_3	b.d	0.00	0.31
Yb_2O_3	0.14	0.46	0.21
FeOt	9.42	1.38	1.67
CaO	0.30	1.36	1.86
F	b.d	0.34	0.56
Total	93.64	87.62	89.67
P	0.180	0.009	0.033
Nb	0.166	0.149	0.004
Si	0.608	0.901	0.958
Ti	0.116	0.011	0.001
Al	0.057	0.019	0.010
Sum B	**1.127**	**1.088**	**1.006**
Zr	0.000	0.267	0.038
Hf	0.000	0.006	0.005
Th	0.534	0.447	0.743
U	0.008	0.015	0.044
Y	0.054	0.076	0.049
La	0.002	0.001	0.003
Ce	0.006	0.005	0.004
Nd	0.008	0.003	0.000
Gd	0.005	0.003	0.009
Dy	0.008	0.006	0.009
Ho	0.002	0.003	0.003
Er	0.000	0.000	0.005
Yb	0.002	0.007	0.004
Fe	0.374	0.056	0.078
Ca	0.015	0.071	0.111
Sum A	**1.017**	**0.966**	**1.103**
Sum	**2.144**	**2.054**	**2.109**

Notes:
1)b.d= below detection limit; 2) n.d.= not determined. Formula calculated on the

Table 7: Representative electron-microprobe analyses and formulae of samarskite-(Y) (ABO_4) and fersmite (AB_2O_6)

Mineral	Sam-Y	Sam-Y	Sam-Y	Sam-Y	Sam-Y		Fers	Fers	Fers
Sample	6490	9827A	9831	9831	9832		4636	9832	9832
Analysis	98*	174	242	243	231*		103*	213	214*
Nb_2O_5	48.32	42.25	47.35	47.44	53.06		45.20	53.23	55.56
Ta_2O_5	0.45	2.73	0.29	0.10	0.61		8.22	3.87	3.76
SiO_2	0.51	0.37	b.d.	0.02	2.25		8.76	0.17	0.14
TiO_2	1.13	1.43	0.31	0.41	1.61		9.51	6.55	6.44
ThO_2	5.13	5.77	1.62	1.85	0.18		1.83	0.34	0.38
UO_2	2.36	3.04	0.69	0.92	0.59		5.75	3.34	3.34
Y_2O_3	22.27	23.69	21.36	21.16	22.27		1.75	0.32	0.27
La_2O_3	0.20	b.d	0.27	0.29	0.35		0.57	1.17	1.30
Ce_2O_3	1.97	0.45	1.98	2.18	2.35		2.56	4.22	3.84
Pr_2O_3	0.30	0.10	0.47	0.55	0.37		0.44	0.43	0.34
Nd_2O_3	2.06	1.36	3.86	4.08	2.35		1.61	1.95	1.59
Sm_2O_3	0.86	0.99	2.16	2.28	0.95		0.47	0.39	0.36
Eu_2O_3	0.06	0.01	0.11	0.17	0.23		0.08	0.17	0.14
Gd_2O_3	2.43	3.66	5.91	5.60	1.98		0.41	0.39	0.26
Dy_2O_3	3.23	3.74	5.75	5.73	2.14		0.38	0.42	0.45
Ho_2O_3	1.10	1.67	2.56	2.56	0.75		b.d	b.d	0.09
Yb_2O_3	2.67	2.92	1.19	1.13	1.30		b.d	b.d	b.d
FeOt	0.43	0.67	0.02	0.09	1.78		0.15	2.53	0.60
CaO	1.30	1.51	0.27	0.27	0.92		10.26	14.37	17.68
F	0.09	0.18	b.d	0.23	0.13		0.21	0.81	0.90
Total	96.79	96.37	96.15	96.84	96.03		97.94	93.85	96.55
Nb	0.993	0.900	1.009	1.006	1.004	Nb	1.384	1.476	1.519
Ta	0.006	0.035	0.004	0.001	0.007	Ta	0.151	0.065	0.062
Si	0.023	0.018	0.000	0.001	0.094	Ti	0.484	0.302	0.293
Ti	0.039	0.051	0.011	0.014	0.051	Fe	0.008	0.130	0.030
Sum B	**1.060**	**1.003**	**1.024**	**1.023**	**1.156**	**Sum B**	**2.028**	**1.972**	**1.905**
Th	0.053	0.062	0.017	0.020	0.002	Th	0.028	0.005	0.005
U	0.024	0.032	0.007	0.010	0.005	U	0.087	0.046	0.045
Y	0.539	0.594	0.536	0.528	0.496	Y	0.063	0.126	0.009
La	0.003	0.000	0.005	0.005	0.005	La	0.013	0.026	0.029
Ce	0.033	0.008	0.034	0.037	0.036	Ce	0.063	0.095	0.085
Pr	0.005	0.002	0.008	0.009	0.006	Ca	0.744	0.944	1.146
Nd	0.033	0.023	0.065	0.068	0.035	**Sum A**	**0.999**	**1.242**	**1.319**
Sm	0.013	0.016	0.035	0.037	0.014				
Eu	0.001	0.000	0.002	0.003	0.003				
Gd	0.037	0.057	0.092	0.087	0.028				
Dy	0.047	0.057	0.087	0.087	0.029				
Ho	0.016	0.025	0.038	0.038	0.010				
Yb	0.037	0.042	0.017	0.016	0.017				
Fe	0.017	0.026	0.001	0.004	0.062				
Ca	0.063	0.076	0.013	0.014	0.041				
Sum A	**0.921**	**1.020**	**0.959**	**0.963**	**0.789**				

Notes:
1)*=analysis with good totals; 2)b.d= below detection limit; 3) n.d.= not determined; 4) Sam-Y=samarskite; 5)Fers= fersmite. Elements calculated in the basis of 4 oxygens for samarskite and 6 oxygen atoms for fermite.

Table 8: Representative electron-microprobe analyses and formulae of aeschynite-(Y) (AB_2O_6) and TiO_2 mineral

Mineral	Aes-Y	Aes-Y	Aes-Y	Aes-Y	Tna
Sample	9832	9832	9832	9832	9832
Analysis	232	236	217	218	237
Nb_2O_5	9.62	6.70	5.06	4.21	2.82
Ta_2O_5	b.d	b.d	0.04	0.21	0.08
SiO_2	4.45	1.73	1.60	1.45	0.12
TiO_2	39.03	42.90	45.36	45.67	91.60
ThO_2	1.33	0.39	0.13	0.17	0.02
UO_2	0.27	0.19	0.13	b.d	0.02
Al_2O_3	0.34	0.07	0.11	0.08	b.d
Y_2O_3	20.10	24.45	25.74	25.17	b.d
Pr_2O_3	0.16	0.05	b.d	b.d	b.d
Nd_2O_3	1.42	0.95	0.68	0.83	b.d
Sm_2O_3	0.95	1.00	0.39	0.61	b.d
Gd_2O_3	4.74	4.43	3.23	3.91	0.04
Dy_2O_3	4.23	4.45	3.69	4.24	0.03
Ho_2O_3	1.78	1.88	1.36	1.60	0.05
Er_2O_3	1.67	1.78	2.85	2.53	b.d
Yb_2O_3	1.53	1.55	2.66	2.57	0.02
FeOt	1.85	1.46	1.43	1.45	1.24
MnO	0.15	0.02	0.05	0.02	0.01
CaO	1.12	0.56	0.42	0.31	0.28
F	0.21	0.06	0.11	0.05	0.01
Total	95.10	94.62	95.03	95.13	96.65
Al	0.021	0.005	0.007	0.005	0.000
Y	0.553	0.681	0.704	0.691	0.000
Pr	0.003	0.001	0.000	0.000	0.000
Nd	0.026	0.018	0.012	0.015	0.000
Sm	0.017	0.018	0.007	0.011	0.000
Gd	0.081	0.077	0.055	0.067	0.000
Dy	0.070	0.075	0.061	0.070	0.000
Ho	0.029	0.031	0.022	0.026	0.000
Er	0.027	0.029	0.046	0.041	0.000
Yb	0.024	0.025	0.042	0.040	0.000
Fe	0.081	0.065	0.062	0.063	0.014
Mn	0.006	0.001	0.002	0.001	0.000
Ca	0.062	0.031	0.023	0.017	0.004
Sum A	1.002	1.056	1.043	1.048	
Nb	0.225	0.158	0.118	0.098	0.018
Ta	0.000	0.000	0.000	0.003	0.000
Si	0.230	0.091	0.082	0.075	0.002
Ti	1.519	1.688	1.752	1.771	0.964
Th	0.016	0.005	0.002	0.002	0.000
U	0.003	0.002	0.002	0.000	0.000
Sum B	1.993	1.944	1.956	1.949	
Total	2.995	2.999	2.999	2.998	1.004

Notes:
1) No=analysis number; 2)b.d= below detection limit; 3) n.d.= not determined; 4)Min=mineral analyzed; 5) Aes-Y= aeschynite -(Y); 6) Tna= TiO_2mineral. Calculations for aeschynite were done in the basis of 2 B-cations and for TiO_2 mineral in the basis of 2 oxygens.

Table 9: Representative electron-microprobe analyses and formulae of hydroxylbastnäsite-(Ce) ($ACO_3(OH)$)

Sample	7658	7658
Analysis	148	149
Ta_2O_5	0.56	0.56
HfO_2	0.81	0.88
ThO_2	3.34	4.43
UO_2	0.43	0.51
La_2O_3	14.30	13.47
Ce_2O_3	29.00	29.99
Pr_2O_3	2.91	2.89
Nd_2O_3	10.25	10.23
Sm_2O_3	1.40	1.45
Eu_2O_3	1.16	1.16
Gd_2O_3	1.27	1.37
Dy_2O_3	0.61	0.59
Ho_2O_3	0.21	0.24
CaO	4.48	4.62
F	0.08	0.11
CO_2-Calc	23.49	23.29
SUM	94.30	95.79
O = F	-0.03	-0.05
Total	99.41	95.96
Th	0.026	0.034
La	0.181	0.168
Ce	0.365	0.372
Pr	0.036	0.036
Nd	0.126	0.124
Sm	0.017	0.017
Eu	0.014	0.013
Gd	0.014	0.015
Dy	0.007	0.006
Ho	0.002	0.003
Fe	0.047	0.042
Ca	0.165	0.168
Total A	0.999	0.999

Notes:
1) No=analysis number; 2)b.d= below detection limit; 3) n.d.= not determined . Calculations were done in the basis of one cation , carbon concentrations were calculated based on charge balance (Ridolfi et al. 2006). Small amounts of Si, Fe, Ti, Al and Mn are also present.

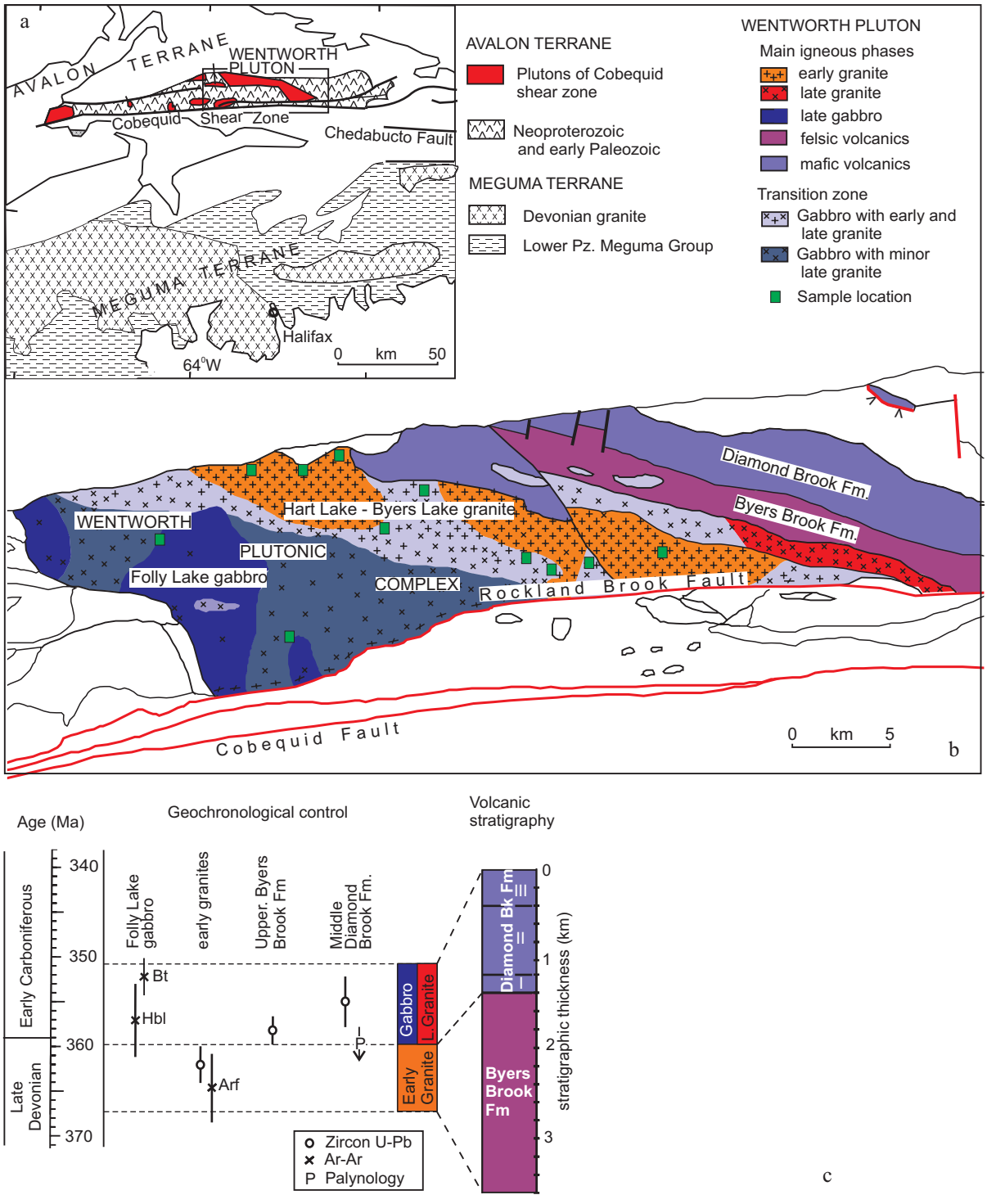
a
AVALON TERRANE
WENTWORTH PLUTON
Cobequid Shear Zone
Chedabucto Fault
MEGUMA TERRANE
Halifax
64°W
0 km 50
AVALON TERRANE
Plutons of Cobequid shear zone
Neoproterozoic and early Paleozoic
MEGUMA TERRANE
Devonian granite
Lower Pz. Meguma Group
WENTWORTH PLUTON
Main igneous phases
early granite
late granite
late gabbro
felsic volcanics
mafic volcanics
Transition zone
Gabbro with early and late granite
Gabbro with minor late granite
Sample location
Diamond Brook Fm.
Byers Brook Fm.
Hart Lake - Byers Lake granite
WENTWORTH
PLUTONIC
COMPLEX
Folly Lake gabbro
Rockland Brook Fault
Cobequid Fault
0 km 5
b
Age (Ma)
Geochronological control
Volcanic stratigraphy
Early Carboniferous
Late Devonian
340
350
360
370
Folly Lake gabbro
early granites
Upper. Byers Brook Fm
Middle Diamond Brook Fm.
Bt
Hbl
Arf
P
Gabbro
L. Granite
Early Granite
Diamond Bk Fm
III
II
I
Byers Brook Fm
0
1
2
3
stratigraphic thickness (km)
Zircon U-Pb
Ar-Ar
P Palynology
c

Figure 1

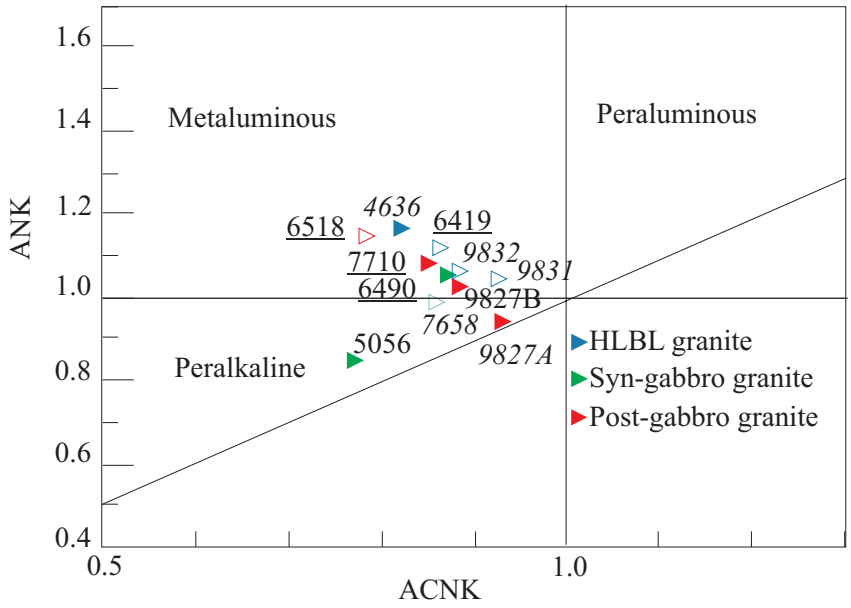
1.6
1.4
1.2
1.0
0.8
0.6
0.4
ANK
0.5
1.0
ACNK
Metaluminous
Peraluminous
Peralkaline
4636
6518
6419
9832
9831
7710
6490
9827B
7658
5056
9827A
HLBL granite
Syn-gabbro granite
Post-gabbro granite

Figure 2

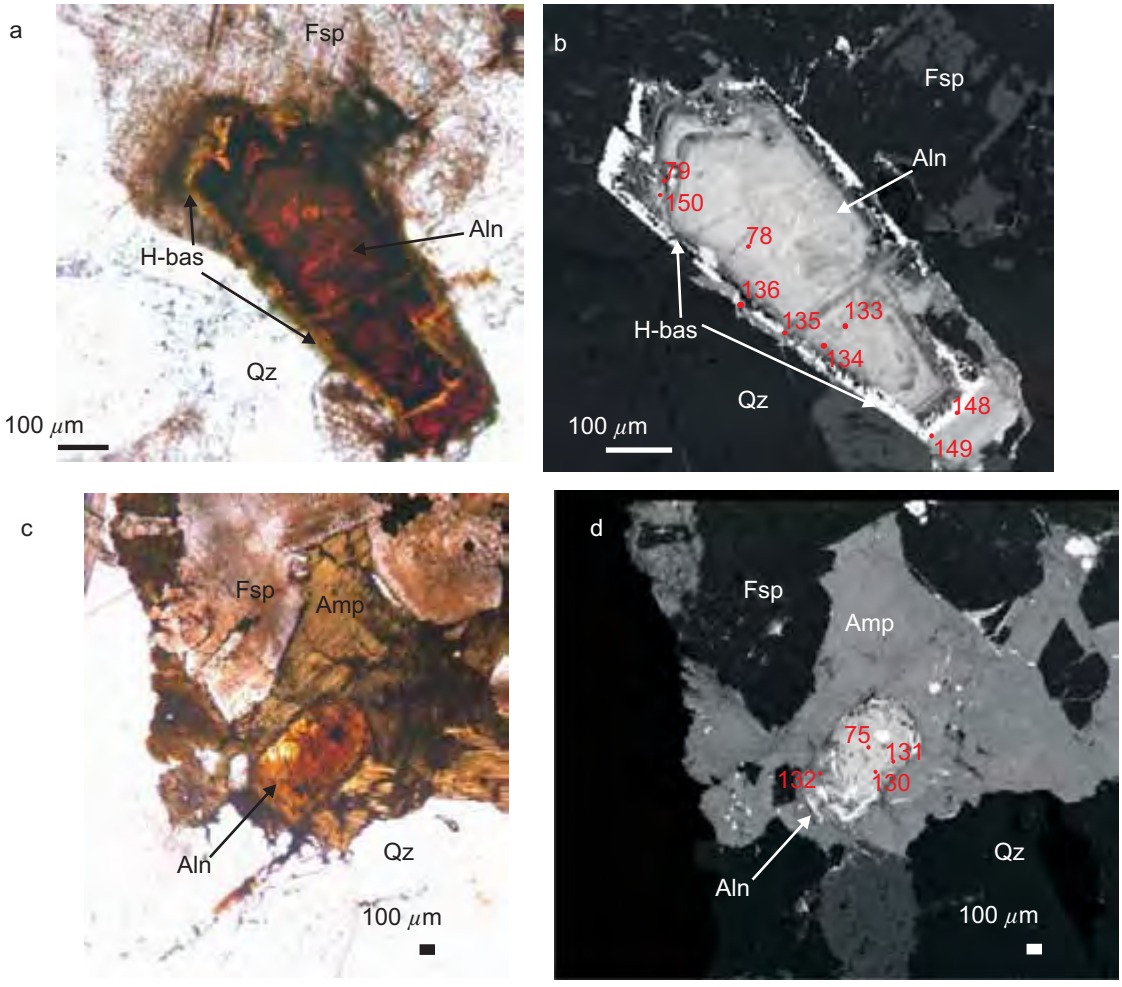
a
Fsp
H-bas
Aln
Qz
100 μm
b
Fsp
Aln
79
150
78
136
135
133
134
H-bas
Qz
148
149
100 μm
c
Fsp
Amp
Aln
Qz
100 μm
d
Fsp
Amp
75
131
132
130
Aln
Qz
100 μm

Figure 3

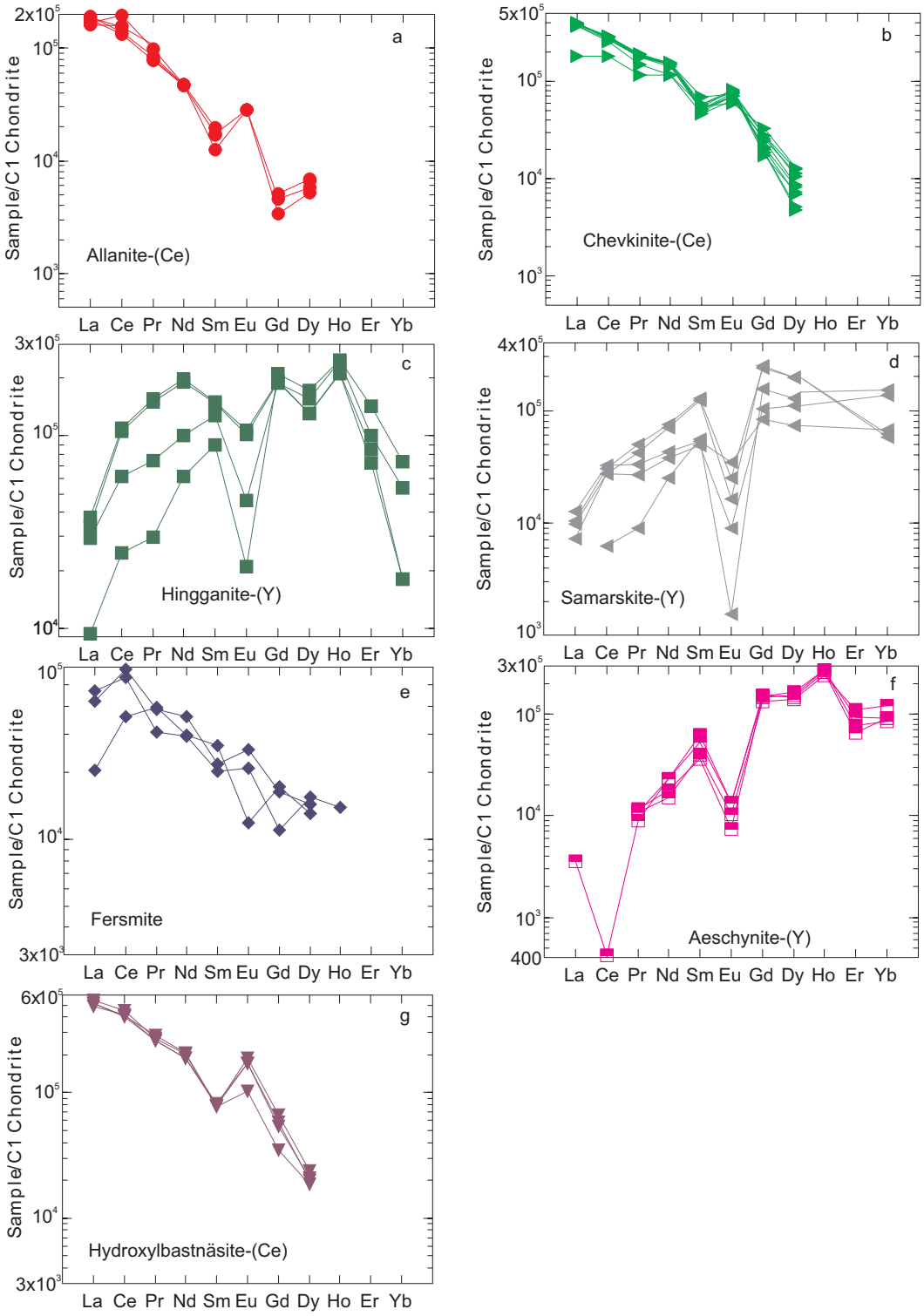
a
Allanite-(Ce)
b
Chevkinite-(Ce)
c
Hingganite-(Y)
d
Samarskite-(Y)
e
Fersmite
f
Aeschynite-(Y)
g
Hydroxylbastnäsite-(Ce)
Sample/C1 Chondrite
La Ce Pr Nd Sm Eu Gd Dy Ho Er Yb

Figure 4

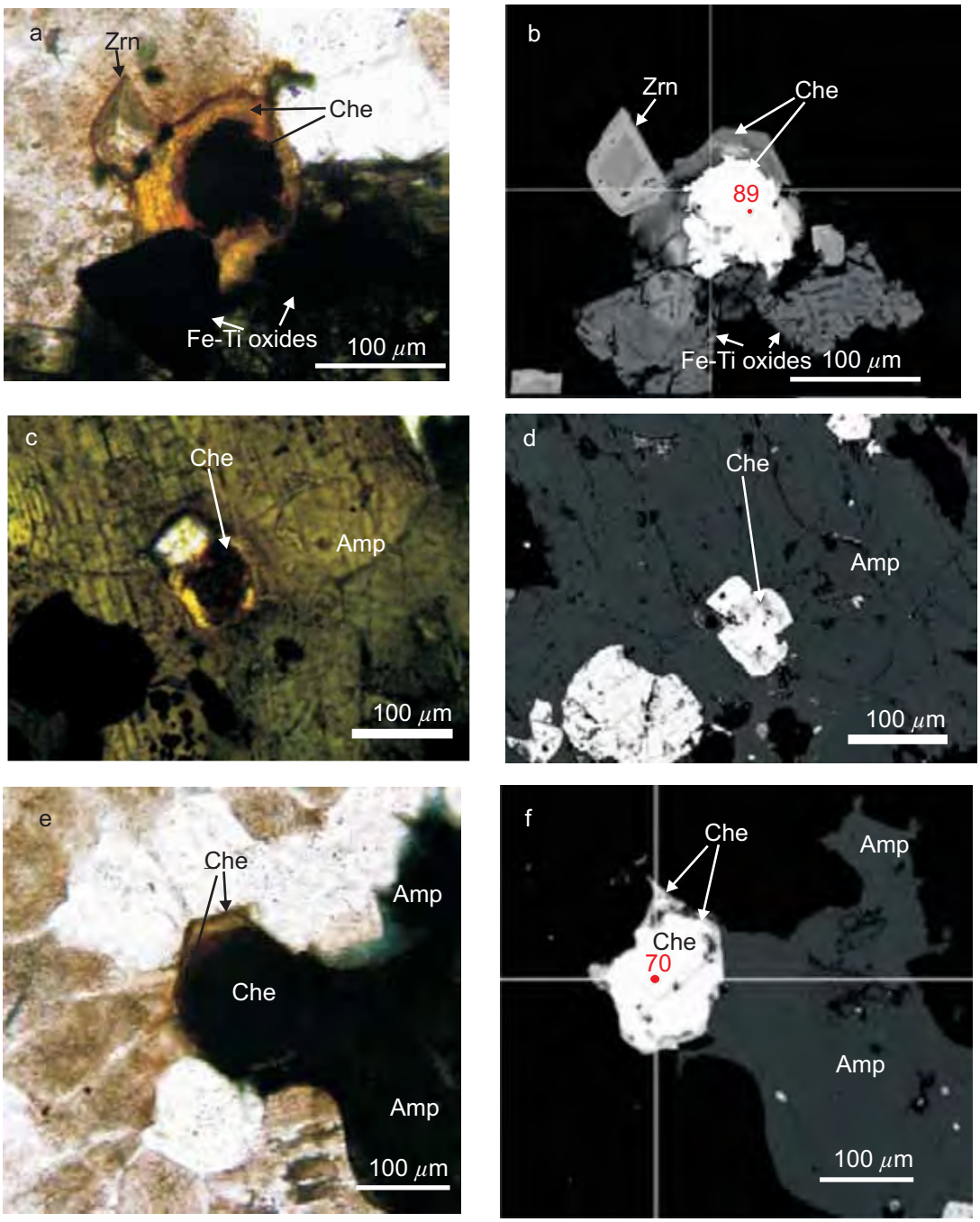
a
Zrn
Che
Fe-Ti oxides
100 μm
b
Zrn
Che
89
Fe-Ti oxides
100 μm
c
Che
Amp
100 μm
d
Che
Amp
100 μm
e
Che
Amp
Che
Amp
100 μm
f
Che
Amp
Che
70
Amp
100 μm

Figure 5

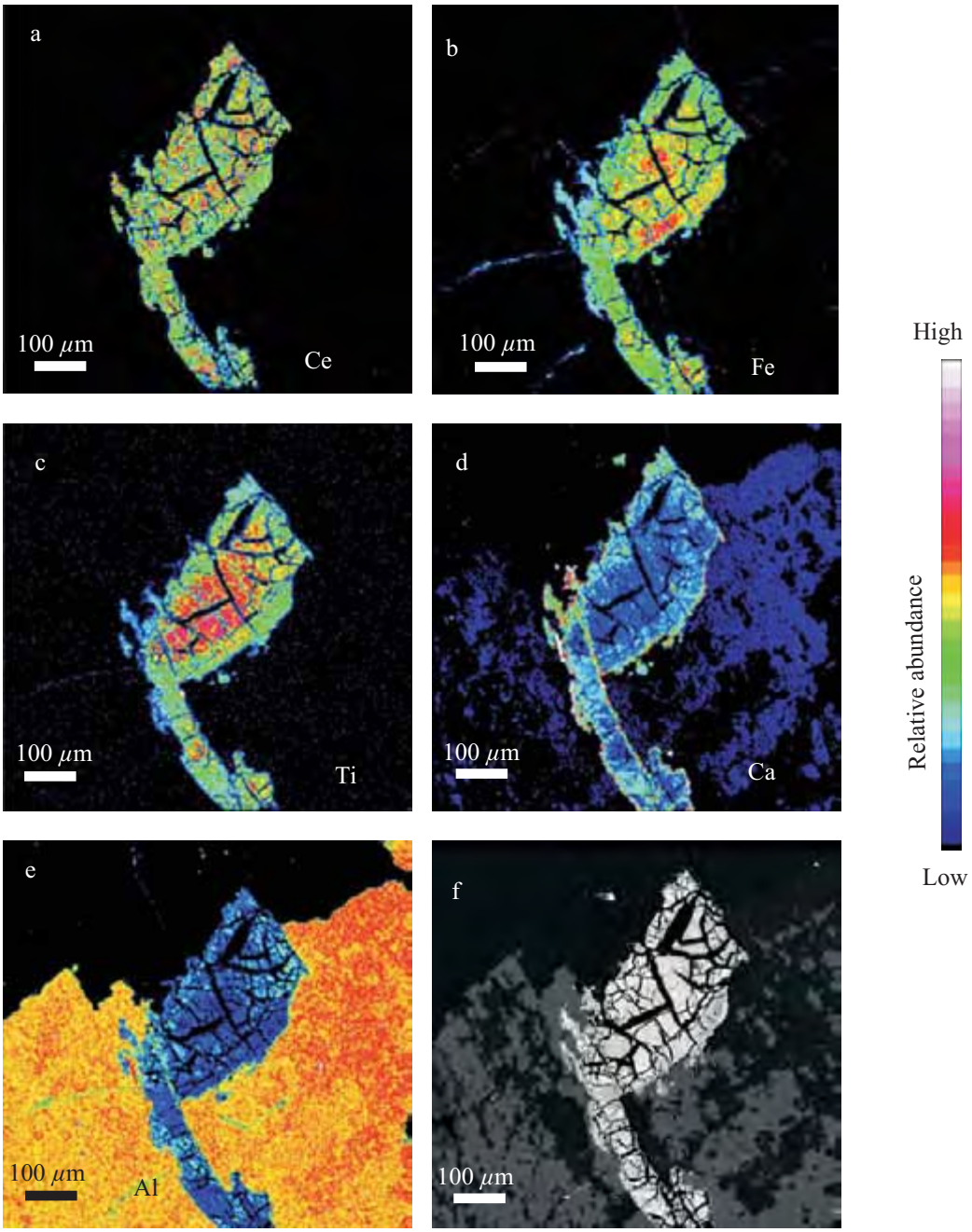
a
100 μm
Ce
b
100 μm
Fe
c
100 μm
Ti
d
100 μm
Ca
e
100 μm
Al
f
100 μm
High
Relative abundance
Low

Figure 6

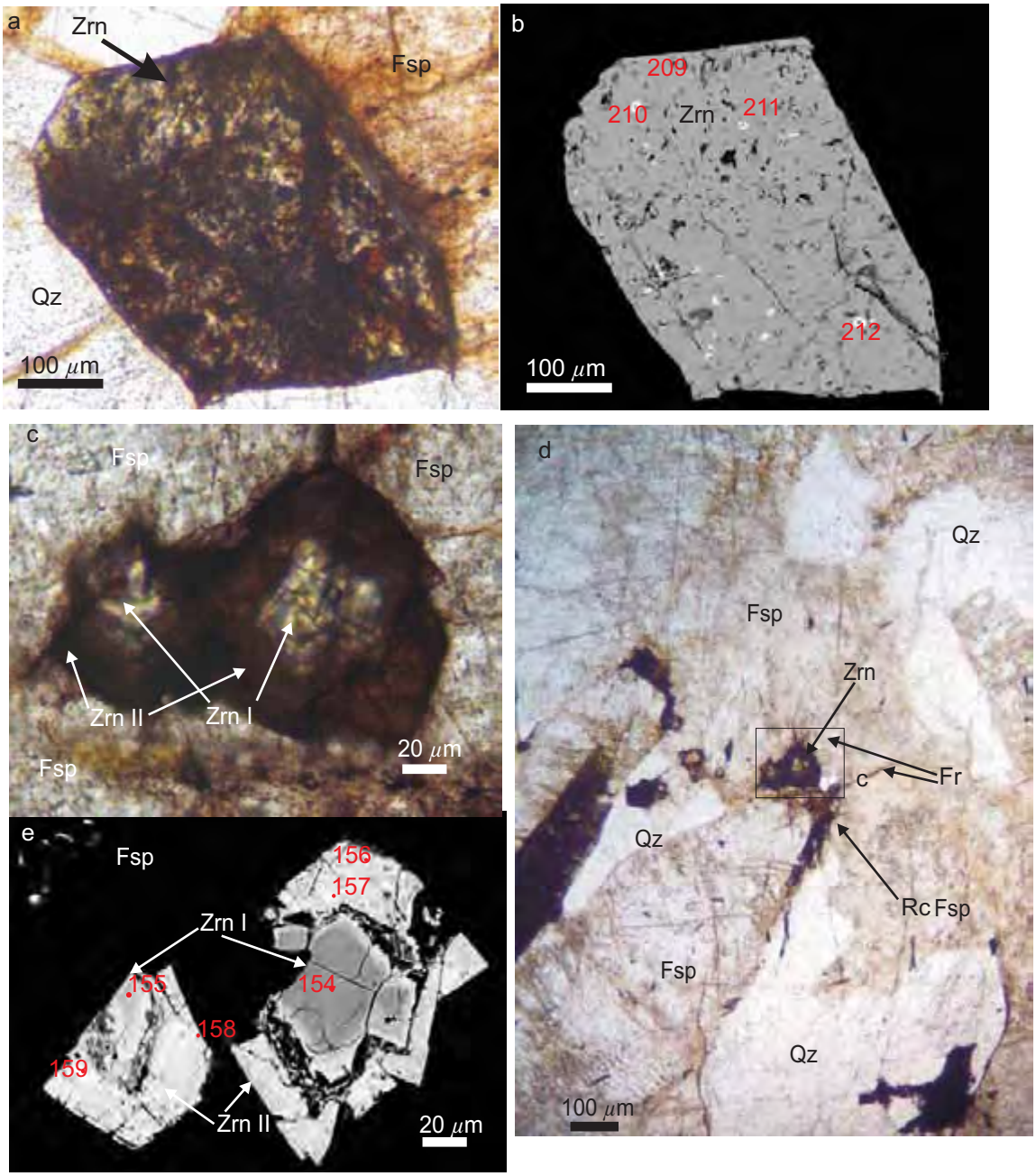
a
Zrn
Fsp
Qz
100 μm
b
209
210
Zrn
211
212
100 μm
c
Fsp
Fsp
Zrn II
Zrn I
Fsp
20 μm
d
Qz
Fsp
Zrn
c
Fr
Qz
Rc Fsp
Fsp
Qz
100 μm
e
Fsp
156
157
Zrn I
155
154
158
159
Zrn II
20 μm

Figure 7

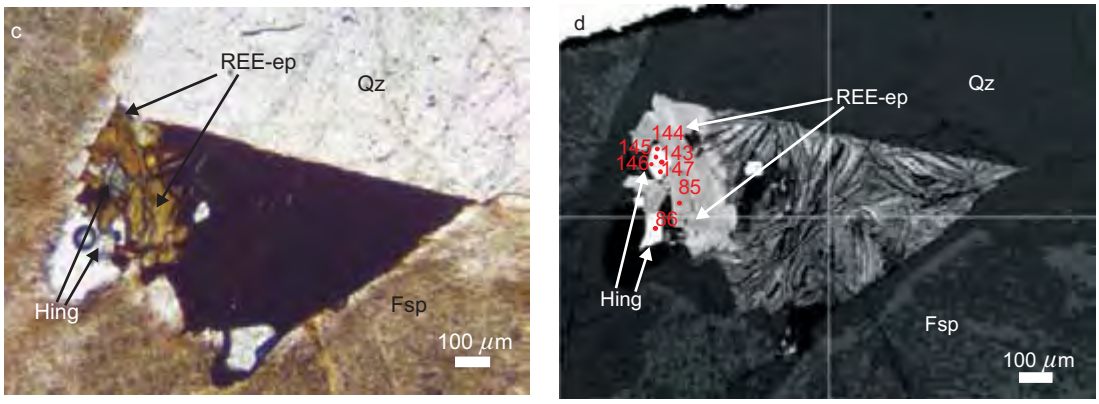
c
REE-ep
Qz
Hing
Fsp
100 μm
d
REE-ep
Qz
144
145
143
146
147
85
86
Hing
Fsp
100 μm

Figure 8

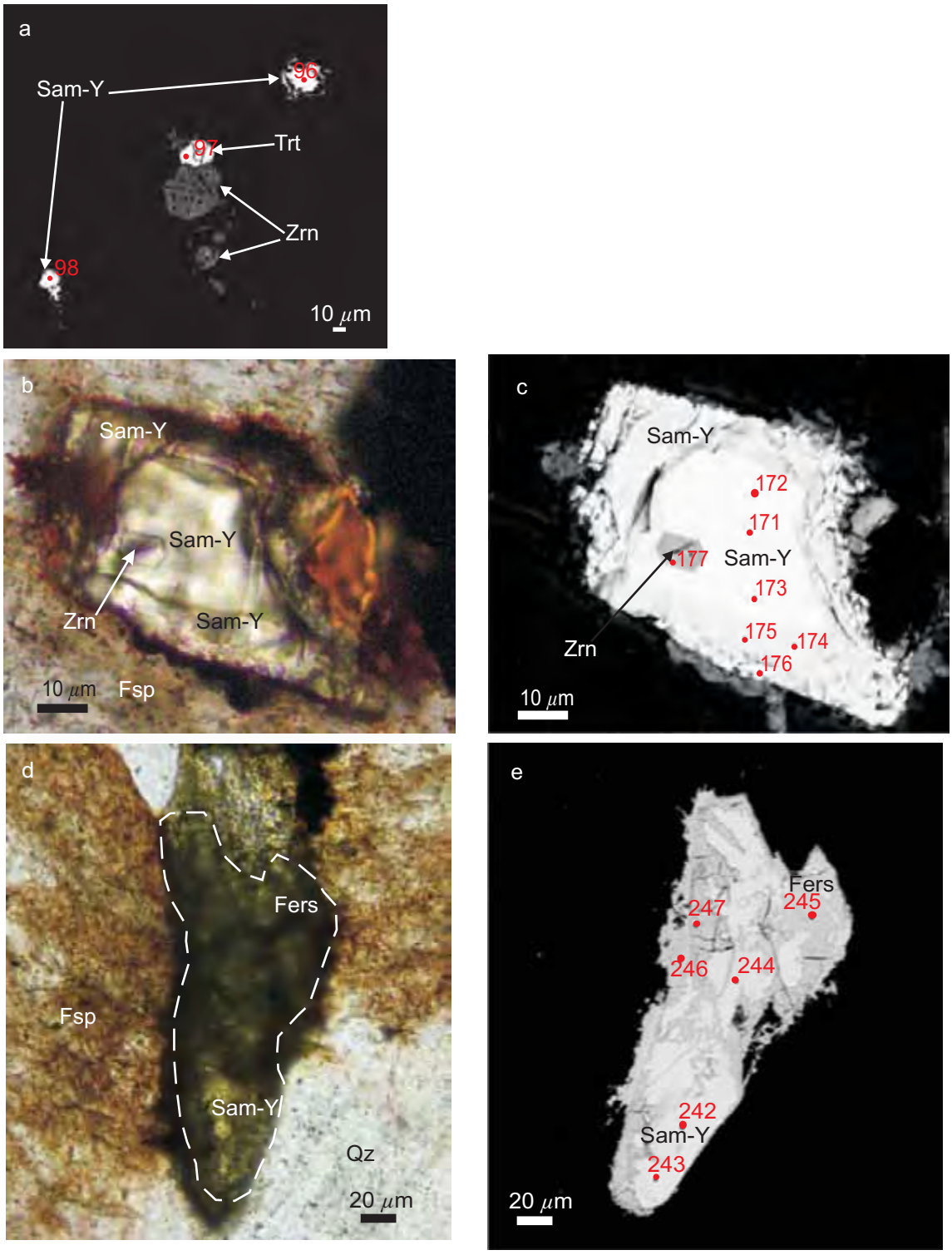
a
Sam-Y
96
97
Trt
Zrn
98
10 μm
b
Sam-Y
Sam-Y
Zrn
Sam-Y
10 μm
Fsp
c
Sam-Y
172
171
177
Sam-Y
173
175
174
176
Zrn
10 μm
d
Fers
Fsp
Sam-Y
Qz
20 μm
e
Fers
245
247
246
244
242
Sam-Y
243
20 μm

Figure 9

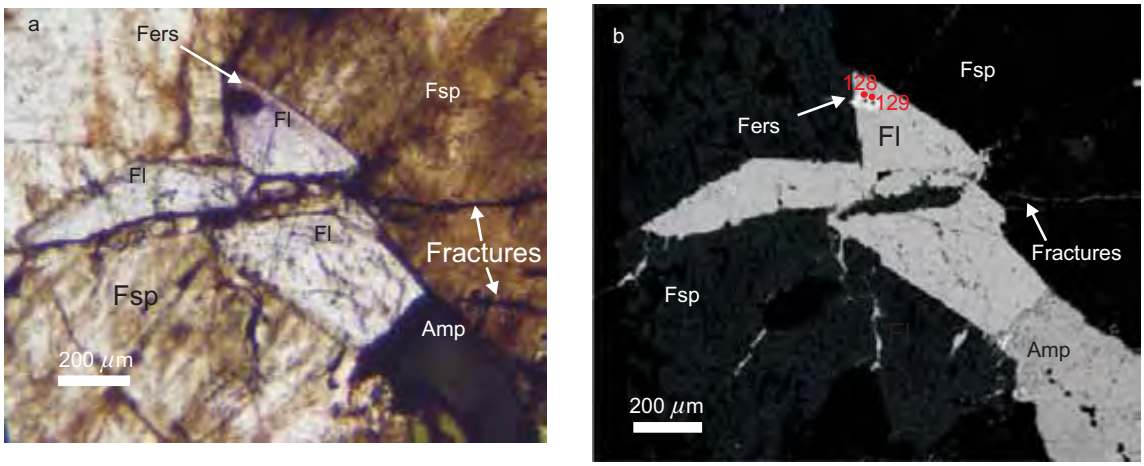
a
Fers
Fsp
Fl
Fl
Fl
Fractures
Fsp
Amp
200 μm
b
Fsp
128
129
Fers
Fl
Fractures
Fsp
Fl
Amp
200 μm

Figure 10

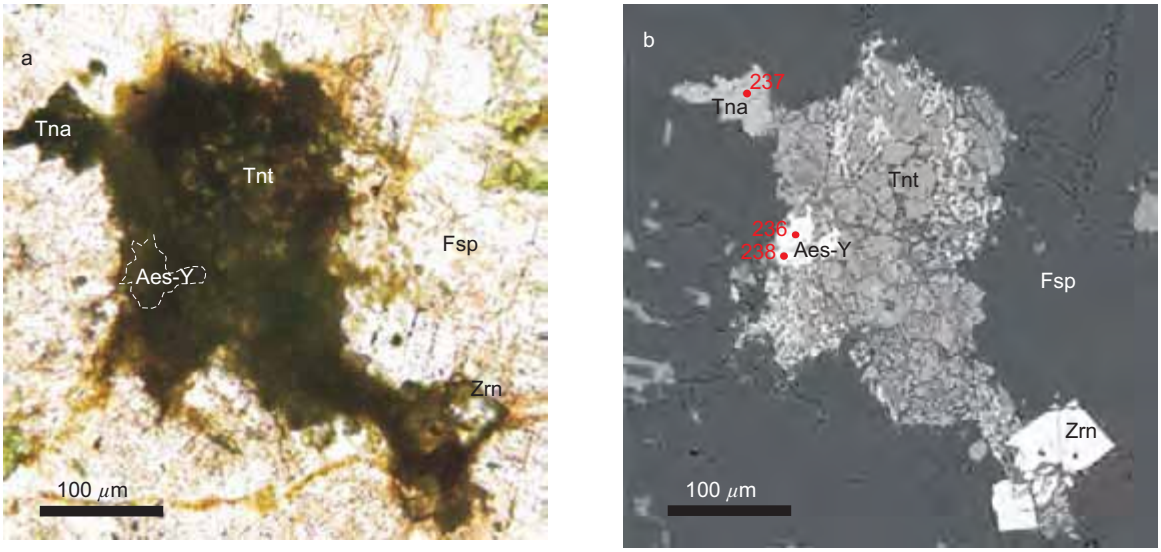
a
Tna
Tnt
Fsp
Aes-Y
Zrn
100 μm
b
237
Tna
Tnt
236
238
Aes-Y
Fsp
Zrn
100 μm

Figure 11

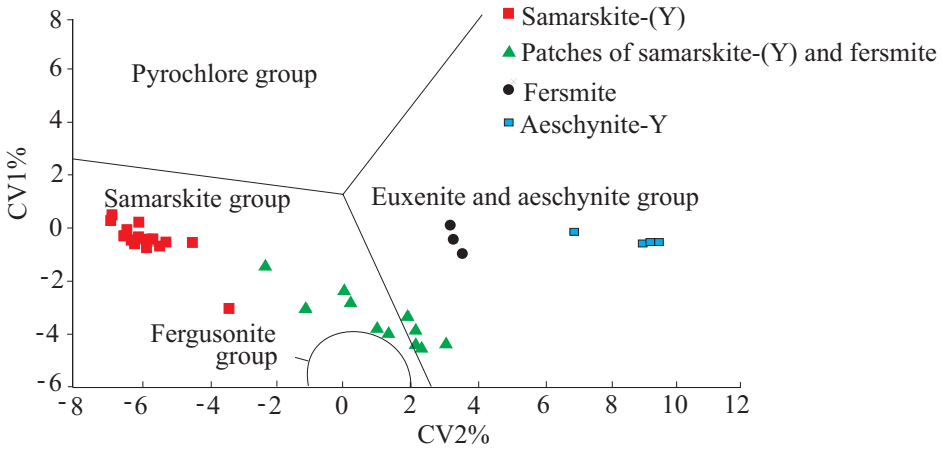
Samarskite-(Y)
Patches of samarskite-(Y) and fersmite
Fersmite
Aeschynite-Y
Pyrochlore group
Samarskite group
Euxenite and aeschynite group
Fergusonite group
CV1%
CV2%
8
6
4
2
0
-2
-4
-6
-8
-6
-4
-2
0
2
4
6
8
10
12

Figure 12

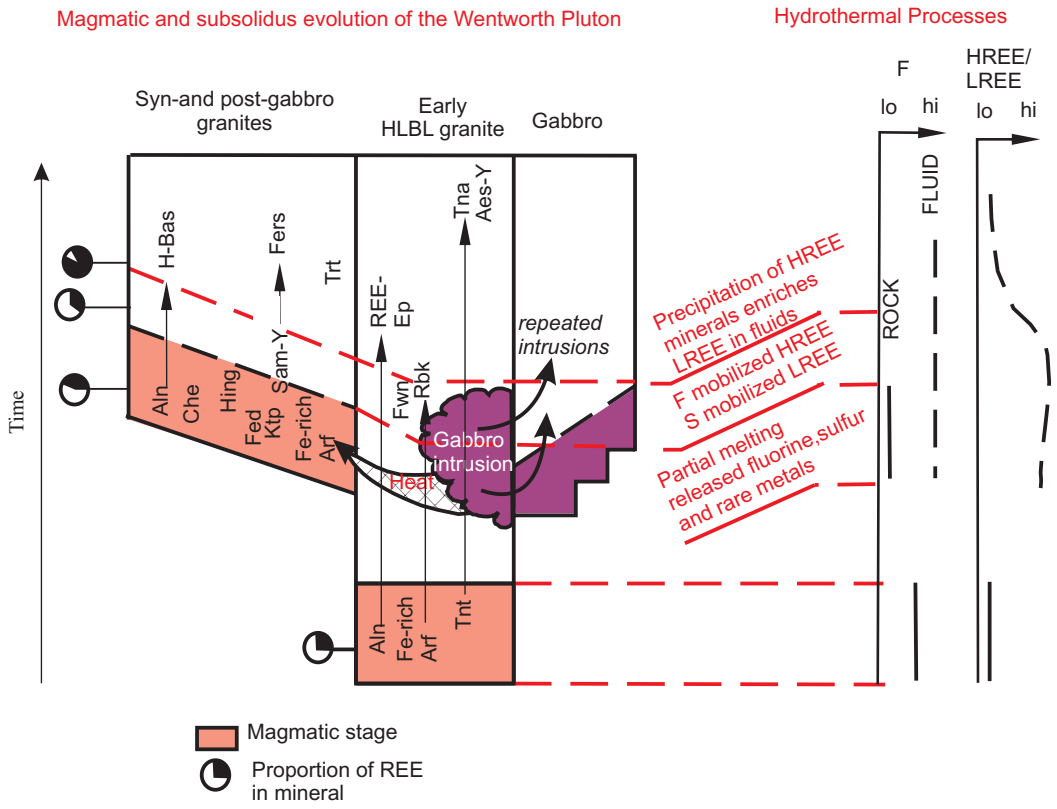
Magmatic and subsolidus evolution of the Wentworth Pluton
Hydrothermal Processes
Syn-and post-gabbro granites
Early HLBL granite
Gabbro
Time
H-Bas
Fers
Trt
REE-Ep
Tna
Aes-Y
Aln
Che
Hing
Fed
Ktp
Sam-Y
Fe-rich Arf
Fwn
Rbk
repeated intrusions
Gabbro intrusion
Heat
Aln
Fe-rich Arf
Tnt
Precipitation of HREE minerals enriches LREE in fluids
F mobilized HREE
S mobilized LREE
Partial melting released fluorine,sulfur and rare metals
F
lo hi
HREE/ LREE
lo hi
ROCK
FLUID
Magmatic stage
Proportion of REE in mineral

Figure 13

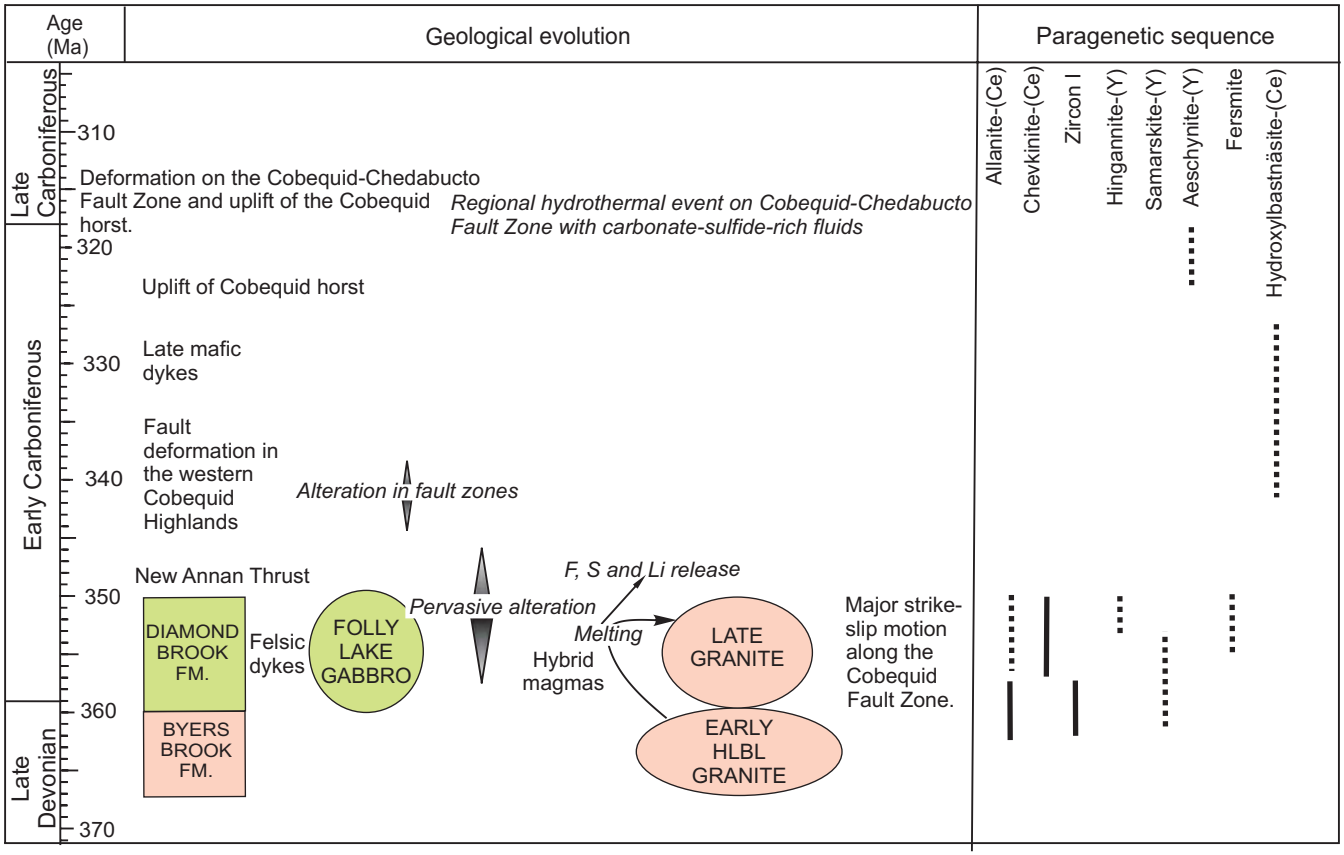
Age (Ma)
Geological evolution
Paragenetic sequence
Late Carboniferous
Early Carboniferous
Late Devonian
310
320
330
340
350
360
370
Deformation on the Cobequid-Chedabucto Fault Zone and uplift of the Cobequid horst.
Regional hydrothermal event on Cobequid-Chedabucto Fault Zone with carbonate-sulfide-rich fluids
Uplift of Cobequid horst
Late mafic dykes
Fault deformation in the western Cobequid Highlands
Alteration in fault zones
New Annan Thrust
DIAMOND BROOK FM.
BYERS BROOK FM.
Felsic dykes
FOLLY LAKE GABBRO
Pervasive alteration
F, S and Li release
Melting
Hybrid magmas
LATE GRANITE
EARLY HLBL GRANITE
Major strike-slip motion along the Cobequid Fault Zone.
Allanite-(Ce)
Chevkinite-(Ce)
Zircon I
Hingannite-(Y)
Samarskite-(Y)
Aeschynite-(Y)
Fersmite
Hydroxylbastnäsite-(Ce)

Figure 14